

CUBESAT SENIOR DESIGN TEAM

SOLAR STEERING: A NOVEL APPROACH FOR CUBESAT ATTITUDE CONTROL

Paolo Arguelles, Kevin Chaput, Steve Kenan,
Dongling Li, Yosuar Vazquez, and Dennis Viveros

May 16, 2018

College of Engineering, Computer Science, and Technology
CALIFORNIA STATE UNIVERSITY, LOS ANGELES

ABSTRACT

Solar sailing is a method of spacecraft propulsion technology using radiation pressure exerted by sunlight on a large reflective surface. An attitude control system is essential for a sail spacecraft to maintain a desired orientation. IKAROS, launched in 2010, practically proved the possibility of using a solar sail as a propulsion system. It also showed the current sail orientation system could change the attitude, but only about 1 degree per day. The goal of this project is to demonstrate the mechanical actuation of solar sails as a novel form of attitude control on CubeSat spacecraft. Open-loop Simulink simulations suggest that the proposed approach can produce up to double the angular acceleration produced by the approach employed by IKAROS. Computer simulations were verified experimentally through the construction of a small-scale wind tunnel, and a scaled down test article demonstrating the attitude control concept. Both open- and closed-loop control was demonstrated in the testing environment. Although further testing still needs to be done, a preliminary wind tunnel test, as well as the aforementioned simulation, builds confidence that this mechanical actuation of a solar sail is not only feasible but has the potential to be the best approach to attitude control using solar wind in space.

Index Terms - *solar steering, CubeSat technologies, small spacecraft, solar radiation pressure, wind tunnel*

CONTENTS

Nomenclature	5
1. Introduction	6
1.1. A Brief History of Solar Sailing	6
1.2. A Brief Discussion of Attitude Control Methods	6
1.2.1. <i>Traditional Attitude Control Methods</i>	6
1.2.2. <i>Attitude Control Methods for Solar Sail Spacecraft</i>	7
1.3. Scope of Work of Proposed Project	7
2. Approach	7
2.1. Design Objective.	7
2.2. Design Process	8
2.3. Organization	8
2.4. Deliverables	9
2.5. Requirements	10
2.5.1. <i>NASA Requirements</i>	10
2.5.2. <i>Envisioned CubeSat Requirements</i>	10
2.5.3. <i>Requirements for Experimental Apparatus</i>	12
2.6. Design Budgets	12
2.7. Risk Analysis	13
3. Attitude Control System Design	15
3.1. Sail Folding Methods	16
3.2. Sail Design Trades	18
4. Proof of Concept Design Build and Test Setup	20
4.1. Payload Integration Setup	20
4.2. Dual Paddle Dynamic Setup.	21
4.3. Testbed Design.	23
4.3.1. <i>Wind Tunnel Test Setup</i>	23
4.3.2. <i>Mechanical Design</i>	25
4.3.3. <i>Electrical Design</i>	29
4.3.4. <i>Test Integration</i>	30
5. Simulation, Test, and Results	
5.1. Simulink Methodology	33
5.1.1. <i>Calculations for the Mechanical Actuation Steering Method</i>	35
5.1.2. <i>Calculations for the Reflectivity Change Steering Method</i>	36
5.2. Computational Fluid Dynamics Model	36
5.2.1. <i>Test Data</i>	37
5.2.2. <i>Calculations for the Reflectivity Change Steering Method</i>	37
5.2.3. <i>Preliminary Results</i>	38

5.3.	Computational Fluid Dynamics Model	40
5.3.1.	<i>Flow Simulation Settings</i>	40
5.3.2.	<i>Flow Simulation Paddle Angles and Mesh</i>	40
5.3.3.	<i>Flow Simulation Goals</i>	40
5.3.4.	<i>Flow Simulation Equation Goals</i>	41
5.3.5.	<i>Flow Simulation vs. Simulink</i>	47
5.4.	Test Data.	48
5.4.1.	<i>Open loop controller data</i>	48
5.4.2.	<i>PID Controller</i>	49
6.	Summary and Conclusions	52
6.1.	Broader Social Impact	53
References		54
Appendix		56

NOMENCLATURE

a_0	Characteristic acceleration
A_C	Total area of the sail light collection
P	Pressure
η	Sail efficiency factor $0.75 < \eta < 0.92$
m_p	Payload mass
m_s	Sail mass
σ_s	Sail - assembly loading
σ	Areal density
ρ_A	Average sail area density
m	Total mass of the vehicle
A_S	Total area of the sail
t	Average thickness of the sail

1. INTRODUCTION

1.1. A Brief History of Solar Sailing

While observing the Great Comet of 1577, a six-year-old Johannes Kepler observed that a comet's tail always points away from the Sun. This observation later led him to theorize that there must exist some kind of "wind" in the otherwise windless environment of space. Inspired by this notion, Kepler wrote in a letter to Galileo, "Provide ships or sails adapted to the heavenly breezes, and there will be some who will brave even that void."^[21]

Scientists now know that Kepler's "heavenly breezes" arise as a result of solar radiation pressure. Thanks to discoveries made by scientists such as James Clark Maxwell, Max Planck, and Albert Einstein regarding the dual wave-particle nature of light and the momentum of massless photons, physicists are able to precisely define the nature of the forces exerted on reflective surfaces in space. Owing to these discoveries, propulsion specialists have conceived of crafts outfitted with "solar sails," reflective mylar screens that provide a surface from which highly energized electromagnetic particles from the sun could bounce, yielding a thrust vector.

Four centuries later, Kepler's idea still lies largely within the realm of science fiction. However, solar sail-based propulsion technologies are slowly becoming more and more prevalent. Three solar sails have successfully deployed in space to date. Japan's IKAROS was the first small-sized spacecraft bus to successfully demonstrate solar sail technology in interplanetary space with its successful deployment which also demonstrated attitude control using the solar wind in May 2010. In December 2010, the NASA's Nano Sail-D2 became the first CubeSat spacecraft to successfully deploy a solar sail in low earth orbit with the Planetary Society's LightSail-1, modeled after Nano Sail D, becoming the second.

Solar sails are currently deemed the most efficient method to achieve interstellar travel. A spacecraft outfitted with ion propulsion technology would take at least two thousand years to reach Alpha Centauri, the nearest star system to Earth. A solar sail is estimated to make the 4.37-lightyear trip in about twenty years, reducing the trip time by two orders of magnitude. The effectiveness of solar sail as a propulsive method is well established; however, using solar wind as a method of attitude control has yet to be proposed.

1.2. Discussion of Attitude Control Methods

1.2.1. Traditional Attitude Control Methods

Spacecraft controllability has long been characterized by a firm reliance on Newton's Third Law of Motion: that a force due to mass accelerated in one direction will produce a force equal in magnitude, and opposite in direction, to the original force. In small spacecraft, slight attitude corrections are usually made by expelling compressed gas from a container inside the chassis. Orbit-keeping and pointing functions are usually performed by reaction wheels and magnetorquers; however, these conventional attitude control systems take up a lot of space and power. This is especially problematic when a payload is constrained by the volume of a spacecraft. In the especially space-restrictive and low-power CubeSat chassis, novel methods for attitude control are given consideration exemplified in this project.

1.2.2. Attitude Control Methods for Solar Sail Spacecraft

Traditional attitude control for solar sailing includes a liquid crystal method, control vane method, and sliding mass method (Figure 1). These are all one-piece configuration solar sails. Spacecraft IKAROS is the example of using liquid crystal method, which through changing the transparency of the liquid crystal that embedded in the solar sail to achieve attitude control. Control vane method is used by a NASA Sunjammer Spacecraft, through changing the degree and the orientation of the control vanes at each edge to achieve steering. Sliding mass method steers through translating the masses along the booms. The movement of the masses creates a different center of mass to allow the spacecraft changing its attitude [18].

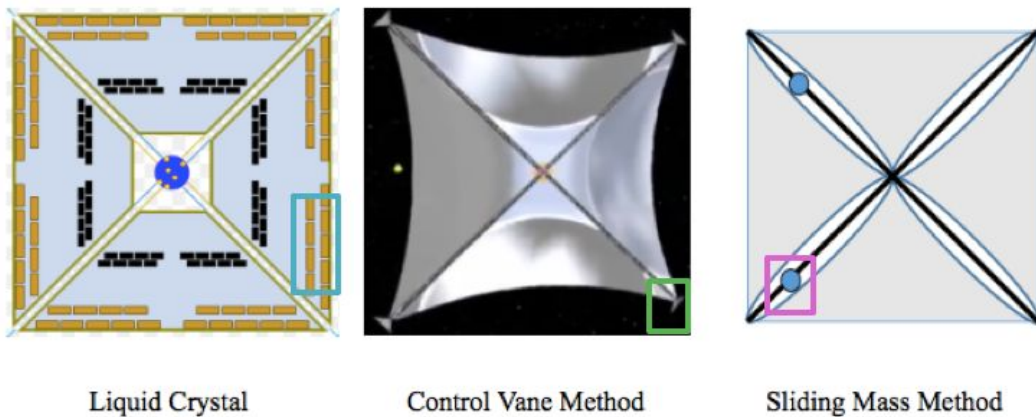


Figure 1. Solar Sail Attitude Control Methods

1.3. Project Scope

This project posits that attitude control may be facilitated by solar-sail inspired technologies utilizing a CubeSat bus. Any serious mission proposing to use this technology should first overcome the apparent gap in simulating or scaling earth to space. One of this project's main objectives is to tighten this gap and demonstrate the feasibility of solar sail-based attitude control which will be referred to as *solar steering* for the remainder of this document.

2. APPROACH

2.1. Design Objective

Two approaches to achieve attitude control using solar sails were considered:

1. **Mechanical actuation** - the use of independently movable vanes that would alter the angle between the solar wind force vector and the normal planar vector.
2. **Reflectivity or emissivity modulation** - the use of electrochromic film to strategically change the reflectivity or emissivity of solar sail vanes or their materials.

The reflectivity approach has been proven by the Japanese Aerospace Exploration Agency with their spacecraft IKAROS, which was able to alter its attitude by 1° per 23 hours. The goal of this novel technology demonstration is to prove the feasibility of the first approach, mechanical actuation.

2.2. Design Process

Two separate sub-teams were formed early on to help streamline this project. The simulation group and the testbed group. The simulation group was responsible for working with Simulink and MATLAB software to design simulations incorporating the forces in the environment that the spacecraft will experience during its mission. The objective of the testbed was to validate the results of the simulations from the various software programs.

Constructing a wind tunnel capable of generating low wind velocities to impart on the sail paddles located on either side of a test article has been the main focus. Each iteration began with rough sketches and dimensional geometries, then computer modeling, lastly the construction of the prototype. For the test article and paddles, a quick prototype was built in order to commence the data acquisition process. As wind tunnel modifications occur, the test article will also undergo modification to find the perfect combination of wind velocity, mass, paddle size, and geometry. Once the final size of the sail paddles was determined, a computer model of the test article was generated to refine the design.

2.3. Organization

The entire project was separated into four groups (Figure 2): testbed design, simulation, administration, and counselors. The objective of the testbed design group was to build a wind tunnel capable of generating weak wind velocities onto the surface of the solar sail panels to test the feasibility of steering. For the simulation group, the aim was to verify calculations using Simulink software. Administration manages individual work properly, and counselors gave advice and supported the project.

Project Organization

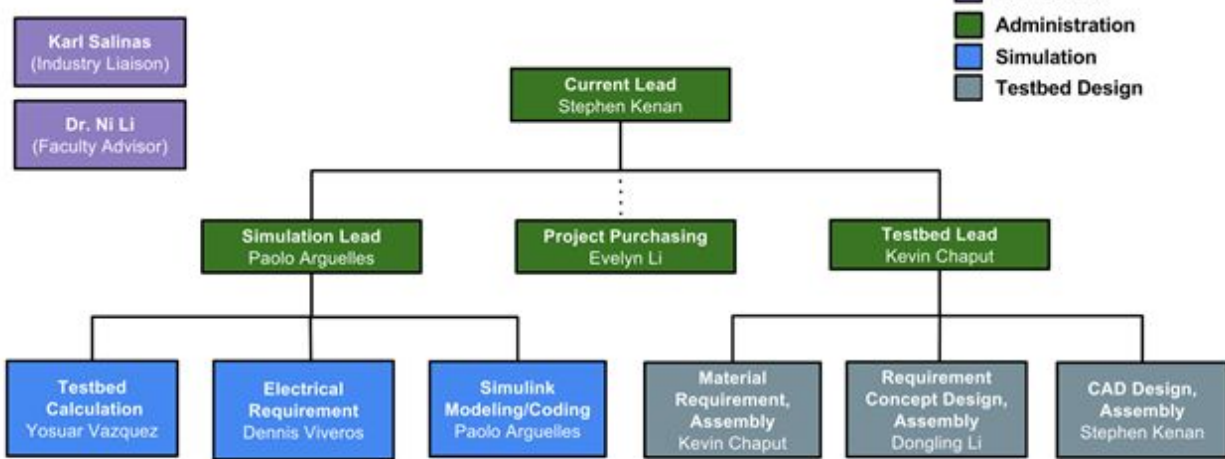


Figure 2. Project Organization Chart.

The contract work breakdown structure (Table A-1) illustrates the breakdown of the four phases of the project and the members responsible for each task. Within each phase are several tasks whose completion were vital in order to move on to the next phase.

2.4. Deliverables

Table 1 summarizes the deliverables that were required throughout the year. The team provided weekly agendas that included meeting minutes, a report and presentation focused on project requirements along with preliminary design concepts, a working testbed, and a final presentation and report with the final design of a test article, data, and test results.

Table 1. Project Deliverables.

Item	Qty	Deliverables Description	Date Required
1	14	Agenda and Minutes	Weekly
2	1	Final Report (Fall)	6-Dec-17
3	1	Final Design Review (FDR)	4-May-18
4	1	Prototype Testbed	4-May-18
5	1	Final Report (Spring)	16-May-18

2.5. System Requirements

Establishing system requirements is paramount to determining mission success or failure. NASA offers research opportunities through programs like the Small Spacecraft Technology Program (SSTP). All technology proposed is gauged at various levels known as technology readiness levels (TRL). TRL ranges from 1 to 9, where 9 is the most mature technology proposed. CubeSat requirements have been honed to meet and stay within NASA constraints of the SSTP. Three requirement sets were defined: (1) NASA requirements; (2) requirements for the envisioned CubeSat; and (3) verifiable requirements for an experimental apparatus, or “testbed,” that will test the solar steering hypothesis. The three requirements sets are shown in Table 2. Each consecutive requirement set was informed by and derived from the previous.

Table 2. Three Requirement Sets

	Requirement Set	Description
1	NASA CubeSat Standard	NASA requirements for small spacecrafts
2	CSULA CubeSat	Requirements governing CSULA CubeSat concept
3	Demonstrator Wind Tunnel + Test Article	Verifiable requirements for experimental apparatus

2.5.1. NASA Requirements

The NASA requirements for small spacecraft, known colloquially as the “CubeSat Standard,” defined a 1-U CubeSat as a small, cube-shaped spacecraft no more than 10 cm on each edge, and less than 1.33 kg in mass. System design will be guided by size, weight, and power (SWaP). Electrical designs will cater to power electronic needs. Power consumption analysis has been notionally predicted for CubeSat and shall be no more than eight watts. Bus voltage will be 12 volts and will be continuously reviewed with further analysis. Both mass and volume of CubeSat are to be maintained under NASA constraints.

2.5.2. Envisioned CubeSat Requirements

Envisioned requirements for an concept CubeSat to act as a technology demonstrator for solar steering are derived from the CubeSat Standard. Given that this design is a 3U CubeSat, it must have dimensions of 10 cm × 10 cm × 30 cm with a mass of no more than 3.99 kg. The envisioned craft is a 3U CubeSat that should operate at altitudes above 900 km; any lower, and the desired effects of solar steering will be cancelled out by atmospheric drag [5].

Table 3. Envisioned CubeSat Requirements

No.	Attribute	Requirements	Capabilities
1	Size	< (10 × 10 × 30) cm	N/A
2	Mass	< 3.99 kg	
3	Power	< 5 W	
4	Altitude	> 900 km	
5	Attitude Control (time for 1° yaw change)	< 1 day	30 mins
6	Solar Sail Size	N/A	25 m ²

Environmental requirements in Table 4 were based on electronic needs and prioritization of efficient solar steering needs. Given that forces are on the micronewton level; atmospheric drag encourages for higher altitudes ranging from 900 kilometers up to 2000 kilometers. Altitudes will make for feasible attitude control, but also demand for industry thermal control designs. A thermal system shall provide adequate operating temperatures for onboard electronics.

Table 4. Environmental Requirements

No.	Title	Requirement	Capability	Verification Method
1	Altitude	Min: 900 km Max: 2000 km	TBD	Analysis
2	Temperature	Min: -20 °C Max: +50 °C	Complies	Analysis

2.5.3. Requirements for Experimental Apparatus

Based on the experimental testbed constructed, there were inherent constraints due to the size of the testbed. Therefore requirements shown in Table 5 were set in place by the team to ensure appropriate sizing of the test article.

Table 5. Experimental Apparatus Requirements

No.	Attribute	Requirements	Capabilities
1	Test Section Dimensions	Base: 0.775 m Height: 0.527 m	Base: 0.58 m Height: 0.395 m
2	Fluid Velocity	< 0.45 m/s (<i>< 1 mph</i>)	0.358 m/s (<i>0.8 mph</i>)
3	Flow Type	Laminar	Laminar and Turbulent
4	Dimensions	(10 × 10 × 10) cm	(7 × 7 × 7) cm
5	Bus Voltage	5 VDC	5 VDC (logic) 4.2 VDC (power)
6	Wireless Capability	RX / TX wireless transmission	RX / TX over Bluetooth Low Energy

2.6. Design Budgets

It was important to keep the size of the mechanical and electrical components as small as possible. This was mainly to ensure a smaller scale test article could be constructed. There were not many hard size, weight, and power (SWaP) requirements in this project aside from being constrained by the size of the wind tunnel. In total, there were three mechanical, and seven electrical components that comprised the test article as seen in Table 7. The battery ended up being a design driver of the test article as it was the bulkiest component at 65 mm wide. The total mass of the components came out to 239.8 grams. This was more than sufficient for test purposes.

Table 6. Component Specifications

Component	Quantity	Dimensions (mm)	Mass (g)
Micro Servo	2	23 × 12.2 × 29	9
IMU	1	20 × 27 × 4	3
PCB	1	53.7 × 35.8	3
Feather 32u4 Bluefruit	1	51.2 × 22.8 × 19.2	8.5
Adalogger	1	51.2 × 23 × 8	5.7
Li-Po Battery	1	51 × 65 × 8	52
Sail Frame	2	250 × 230	50
Test Article Frame	1	70 × 70 × 70	140
Total	10		239.8

Components constructed from non-space flight materials would most likely be used to develop the prototype without the sensitivity to mass. Later down the road, more advanced, expensive space flight materials will be used inflight integration and testing and will have to work as designed with the power and geometric architecture. A good baseline SWAP budget may consist of the basic constraints, such as the actual 3U bus. The final spacecraft also has a gross mass constraint of 3.99 kg which is important to keep in mind. The current test article is only at a stage that includes reasonable components and not at the stage of design of actual payload. Ergo there is no official design budget at this time rather only notional.

2.7. Risk Analysis

Risks were divided into both technical and schedule based (Table 7). No budget risks were considered as the project was heavily research focused. Risks were assessed from low to high based on consequence and likelihood. Mitigation approaches were properly allocated for each risk. Fan failure has been assessed as high risk due to the high cost and lack of a replacement one. Communication and sensor failure were less likely to happen yet would have caused the same type of consequence. Vigilant and frequent simulation testing allowed enough data analysis to avoid such events. Hardware and software issues were considered and assessed a medium high risk concern; problems were avoided by significant breadboard testing. Wind tunnel readiness (line item 9) caused the most delay due to constant modification and lead time for parts. A full list below with risk assessments of probable project delays. Figure 3 illustrates

the consequence of each risk. Table 7 lists the risk item, mitigation approach, and probability of delays.

Table 7. Risk Assessment Chart.

No.	Risk Item	Mitigation Approach	Con •	Prob •	Risk Assessment
<i>Technical Risks</i>					
1	Software design delays	Increase personnel contributions	4	2	MEDIUM
2	Mechanical design delays	Increase personnel contributions	4	1	MEDIUM
3	Hardware/software interface issues	Breadboard testing	5	2	MEDIUM HIGH
4	Communication failure	Frequent simulation testing	5	2	MEDIUM HIGH
5	Sensor failure	Frequent simulation testing	5	2	MEDIUM HIGH
6	Battery failure	Fully charged Lithium-ion	5	1	MEDIUM
7	Fan Failure	Vigilant input voltage monitoring	5	3	HIGH
8	Temperature effects	Logical design of component layout	2	1	LOW
<i>Schedule Risks</i>					
9	Wind tunnel readiness	Increase personnel contributions	4	2	MEDIUM
10	Change in requirements and project scope	Increase personnel contributions	5	1	MEDIUM

		CONSEQUENCE OF RISK				
		Low 1	Minor 2	Moderate 3	Substantial 4	Severe 5
Likelihood	>70%					
	30-70%					
	10-30%					7
	1-10%				1, 9	3, 4, 5
	<1%		8		2	6, 10

Figure 3. Consequence of Risk Chart.

3. ATTITUDE CONTROL SYSTEM DESIGN

The main mechanical components to this CubeSat are the sail membrane, deployment booms, and arms connecting the sails to the payload. Each one plays a pivotal role in the success of the mission and must be carefully considered before making a final decision. Seeing as how many of the following options have already been used in spaceflight, there are merits to each. Each mission and application is different from the previous and has its own set of requirements.

On the other hand, the new design has four individual sails that are attached by beams, and the beams are connected to rotating motors. By changing the orientation of the sails, it accommodates the radiation pressure ratio on the solar sail to maneuver the overall CubeSat. With the usage of mechanical actuation, this method of steering is more efficient than the method used by IKAROS.

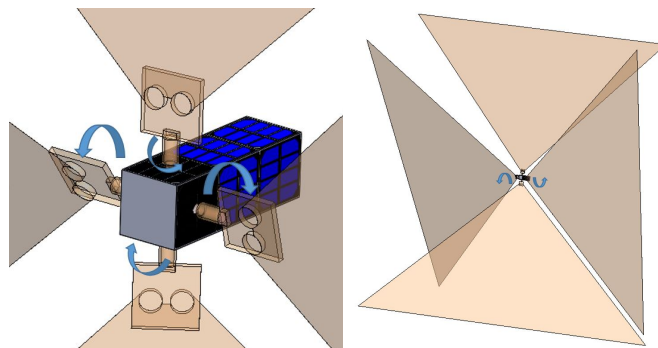


Figure 4. Close-Up View (left) and Full View of New Solar Sail CubeSat Design (right)

3.1. Sail Folding Method

Due to the limited storage for solar sail, it is extremely critical to have a better folding method to storage large area of solar sail. Out of all the research and experiment, herringbone and frog leg folding method were selected as the optimal candidates for solar sail folding.

Herringbone, shown in Figure 5, has a characteristic of repeating in the zigzag pattern, and it allows for extending and retracting the pattern in both directions. This capacity is used to build solar sails for satellites that could be tightly packed, and it has the maximum extension once unfolded^[17]. However, it is not recommended folding into a rectangular shape, and folding it two directions into a small piece would be a challenge. On the other hand, frog leg folding can be a better candidate compared to herringbone method, shown in Figure 6, because of its high efficiency and strong deployment performance, for it allows minimal storage volume and allowing controlled sail release^[19]. Meanwhile, based on the frog leg folding, instead of packing it horizontally, folding vertically provides more room for the sail, shown in Figure 8. This method was also implemented by LightSail from The Planetary Society^[16]. With the zigzag folding method, the base area of the sail can fold to 1/625 of its original shape where it stores inside the sail enclosure. See Figure 9 and Figure 10.

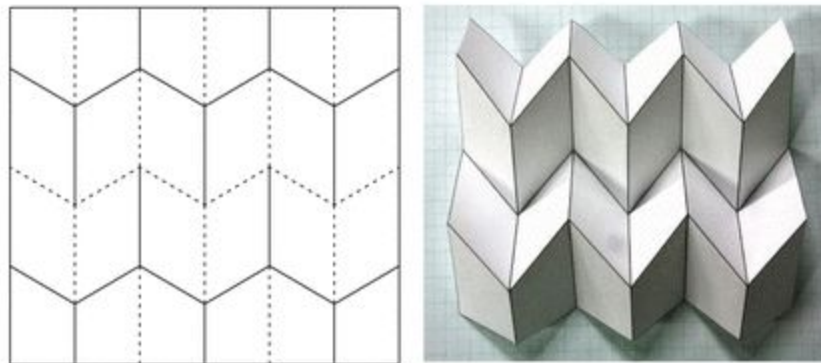


Figure 5. Herringbone Folding

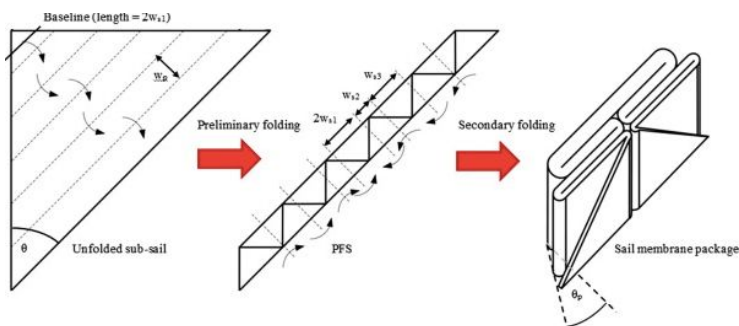


Figure 6. Frog Leg Folding

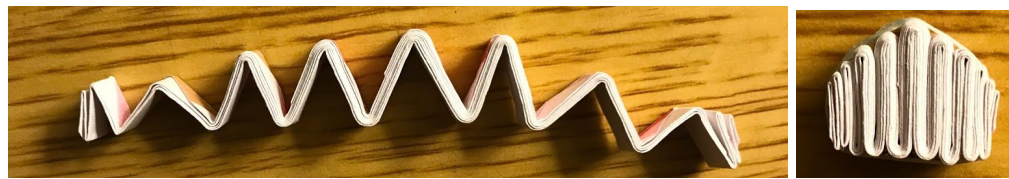


Figure 7. Zigzag Folding



Figure 8. Sail Enclosure and Extended Sail

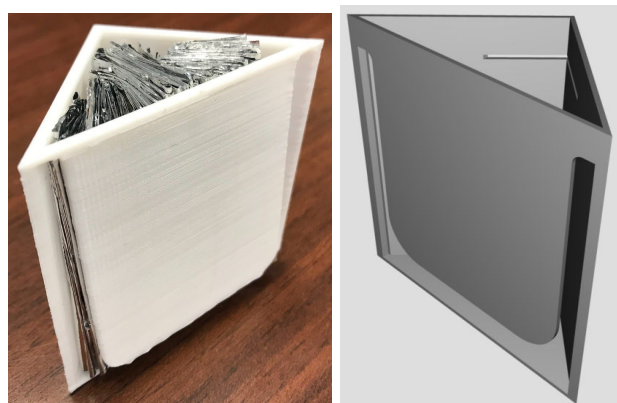


Figure 9. Sail Enclosure

Figure 10 shows the process of deploying a 1.75 meter base and 0.875 meter height solar sail. Two ends of the sails are pulled along with each side of the sail enclosure, which forms a 90 degree angle that simulates the deployment of the boom.

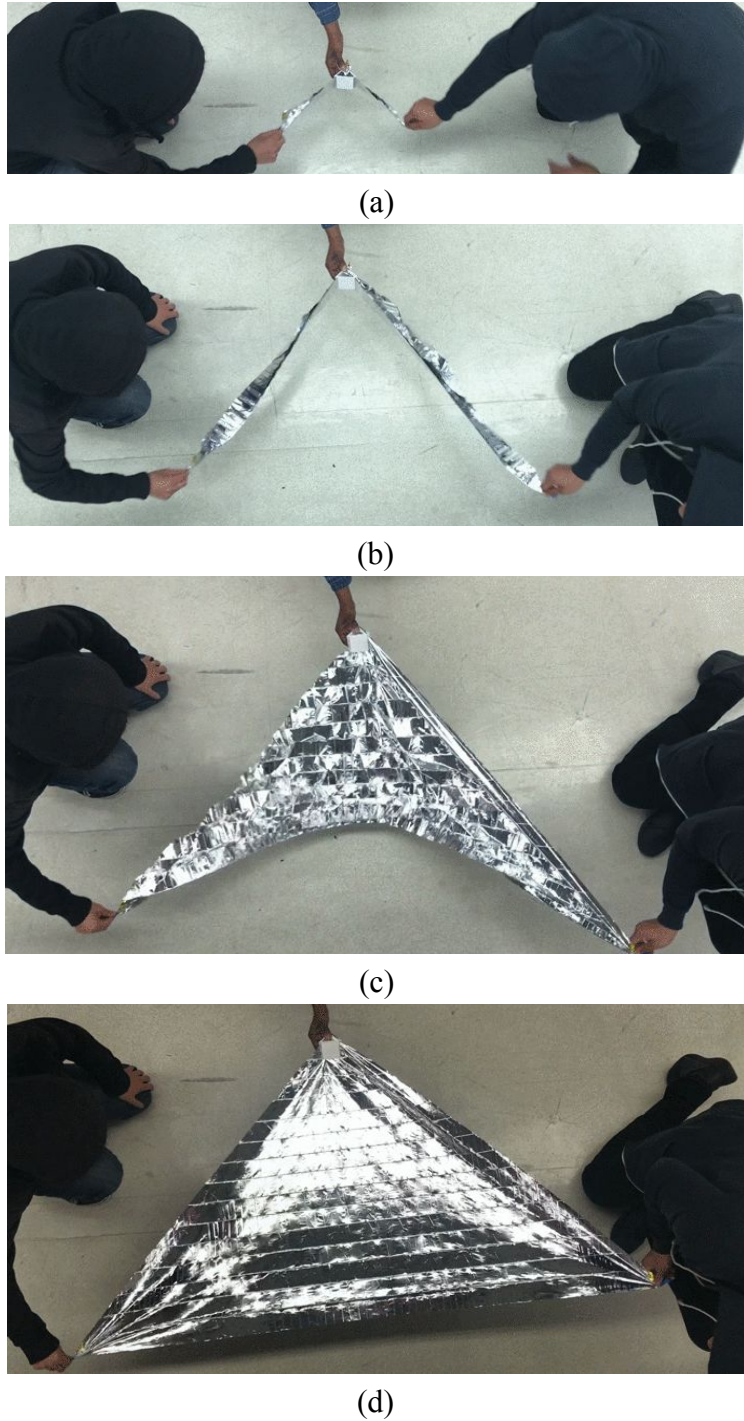


Figure 10. (a) to (d) Space Blanket Deployment (Mylar)

3.2. Sail Design Trades

Taking a look at sail membrane candidates, there are three types of membranes being employed in modern solar sail spacecraft, Mylar, Kapton, and CP-1 (Figure 4). Mylar, which is a Polyethylene polymer based material. Kapton and CP-1 are made of Polyimide, which is a blend

of imide polymers that are more heat tolerant than Mylar. All are polymer based materials but differ slightly in their chemical makeup. All three candidates, as long as they include a Chromium backing layer, have identical reflectivity and emissivity. After weighing all the key aspects in a trade study , shown in Table 9, it was determined that the best option would be the aluminized mylar due to its thinness and lowest density out of all the candidates. Also, since this mission would be taking place in Low Earth Orbit, the need for higher heat tolerant material isn't critical. However, it is noted that Kapton can better maintain its properties at extreme temperatures, which could be the superior choice for future deep space missions.

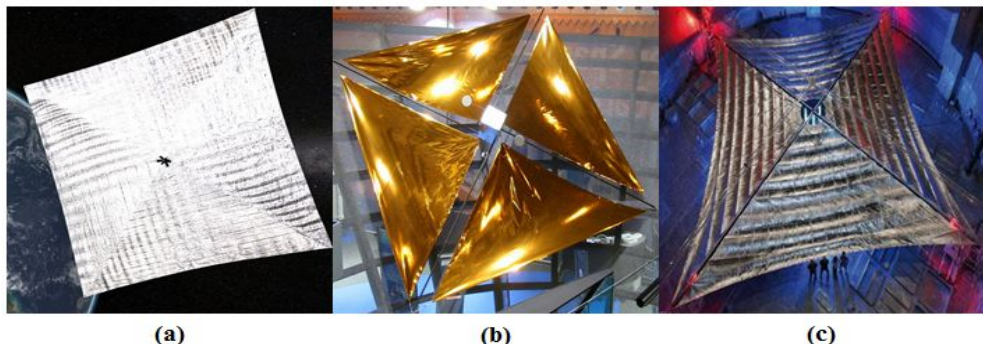


Figure 11. (a) Mylar.^[17] (b) Kapton.^[5] (c) CP-1 Sail Membrane Options.^[12]

Table 8. Sail Membrane Trade Study.

	Option 1	Option 2	Option 3
Type	Aluminized Mylar (Chromium backing)	Kapton (Chromium backing)	Aluminized CP-1 (Chromium backing)
Thickness (μm)	0.9	2	2.5
Density (g/cm ³)	1.39	12	6
Reflectivity	0.88 - 0.9	0.88 - 0.9	0.88 - 0.9
Emissivity	0.63 - 0.73	0.63 - 0.73	0.63 - 0.73

Regarding the deployment process of the sail membrane, there are different mechanism assemblies available. First, the Triangular Rollable and Collapsible (TRAC) boom that takes on a triangular shape upon deployment. Second, is the Collapsible Tube Mast (CTM) which takes on a lenticular shape upon deployment. Each is flattened and tightly wound on a storage spool and then telescopes out into their respective cross-sectional shapes. The stored strain energy of the rolled booms furnish the driving force to simultaneously deploy the booms and sail membrane. Figure 5 illustrates the distinct shape of each mechanism type.

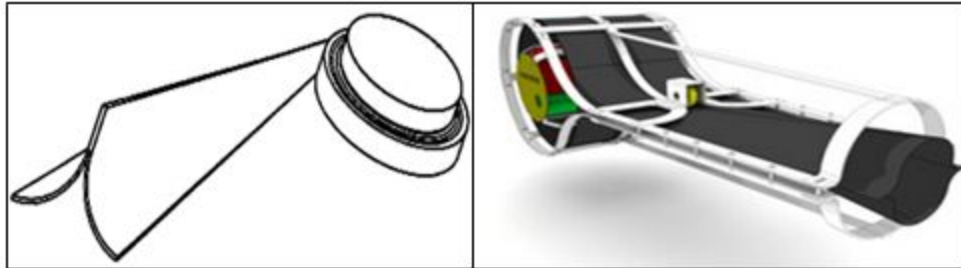


Figure 12. (a) TRAC Boom.^[2] **(b)** CTM Boom.^[11]

Since space is at a premium on a CubeSat, based on the trade study shown in Table 10, the TRAC boom appears to be the optimal choice for this application. It's more compact, has less mass, and a higher second moment of area compared to the CTM boom. Air Force Research Lab tests have shown that the TRAC boom has a higher second moment of area, which is a measurement of how efficient a cross-sectional shape is to resist bending caused by loading, than the CTM boom.^[1]

Table 9. Deployment Boom Trade Study.

	Option 1	Option 2
Type	TRAC	CTM
Method	Telescoping	Telescoping
Form Factor	3U, 6U, 9U	3U, 6U, 9U
Dimensions (cm)	$1.9 \times 1.9 \times 2.32$	$11 \times 11 \times 15$
Mass (kg)	0.46	2
Second Moment of Area (m^4)	4.99×10^{-10}	4.81×10^{-11}

4. PROOF OF CONCEPT DESIGN BUILD AND TEST SETUP

4.1. Payload Integration Setup

The research on payload requirements and capabilities of the Attitude Control Solar Sail, had already come a long way. So what was the starting point for the design of spacecraft that is so elegant? The biggest challenges in the design of a spacecraft on Earth are air and gravity. The testbed for this would be massive and there are no current ways of how to simulate solar wind on earth! Given the constraints of this project, scaling earth to space would be too large of an undertaking. Not only is there no turbulence or atmospheric drag in space, but the theoretical math that attempts to explain solar radiation pressure alone is mind boggling.

Upon the establishment of the “Big Picture” of the mission, motion can be made towards the new design concept. To develop a strong foundation for understanding and having a clear picture of the physics involved, a deep dive into the vast theoretical science of solar sailing must be taken. The formulas often included, but were not limited to the following: characteristic acceleration, areal density, payload mass fraction, and mass flow rate. Despite taking place in outer space, this has quickly become a problem in aerodynamics.

Characteristic Acceleration
$$a_0 = \frac{2\eta P}{\sigma_S + (\frac{m_P}{A})} \quad (1)$$

Areal Density
$$\rho A = \frac{m}{A} \quad (2)$$

Solar Radiation Force
$$F_D = \frac{1}{2}v^2 C_D A \quad (3)$$

Pressure with Drag
$$F_D = \frac{1}{2}v^2 C_D A \quad (4)$$

The research went from everything from solar radiation pressure and spacecraft attitude control to the aforementioned CubeSat standard and solar sail design. First there at least needed to be some simple empirical vision of how the tight payload would integrate into the available volume with all of the other subsystems. So to envision the final spacecraft, a 3U CubeSat Bus with perhaps a tape spring boom deployment system with mechanical louvers shown in Figure 13 or perhaps a design much more elegant.

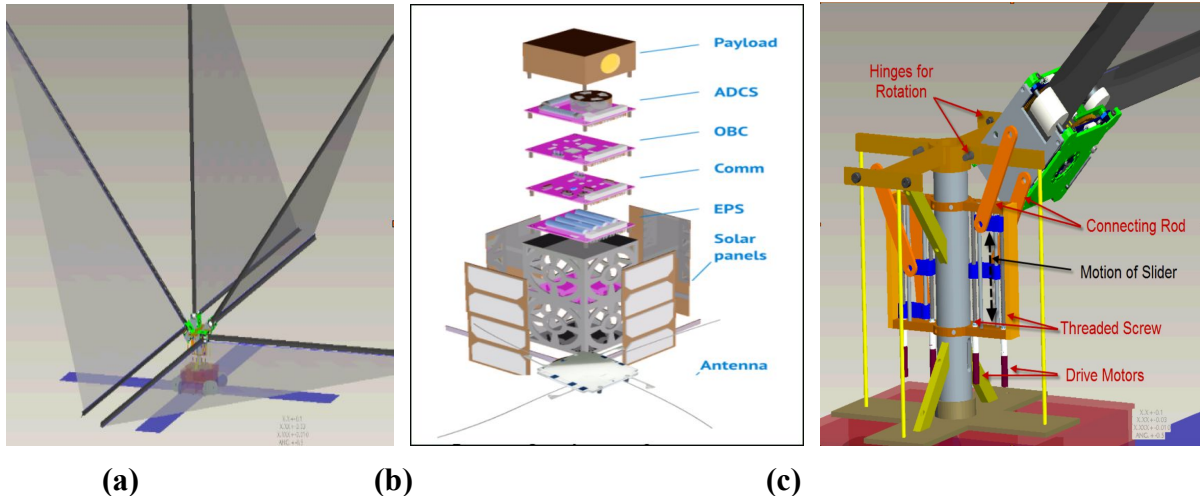


Figure 13. (a) Feathersail, The Next Gen Nano-Class Sail Vehicle. (b) 3U Example of Available Payload Volume. (c) Feasible Stow and Deploy Steering Mechanism^[5]

4.2. Dual Paddle Dynamic Setup

A preliminary One Degree of Freedom (1DOF) system was developed first using a single paddle configuration in Figure 14a to check feasibility and have an early on visualization of any stops that may be encountered. This intuitive test yielded absolutely no useful data but did lead to the obvious conclusion that a minimum of two paddles would be needed. It was previously

concluded that mechanically actuated sails would be a very advantageous way to achieve solar steering, but this would be too complex of a testbed. It was therefore found that a simple dual paddled proof of concept, test article as in Figure 14b would be needed to start testing.

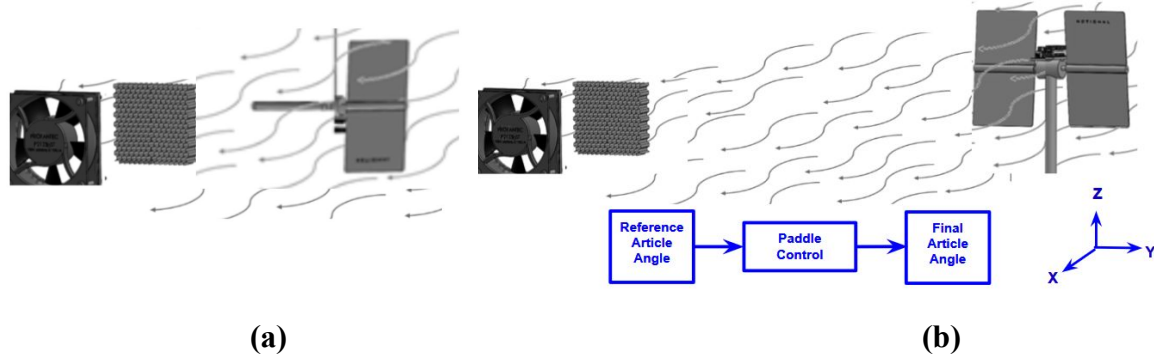


Figure 14. (a) Single Paddle Set-Up. **(b)** Double Paddle Set-Up with Open-Loop Design.

A design concept being considered down the road is shown in Figure 15a. In this design, there would be two panels housing all the mechanisms on either side that would unfold. Then two booms and constant force springs per panel would telescope out and deploy simultaneously unfurling the sail. In order to apply constant tension on the sail, the springs exert a nearly constant restraining force to resist uncoiling and would run along the outside of the booms. Building on design concept 2, Figure 15b illustrates a payload incorporating a sail mast. This design option would have the two panels housing all the mechanisms on either side that would unfold. However, this design would begin with a mast with the sail membrane deploying like an accordion. Once it locks into place, the mast would rotate along with the telescoping booms and constant force springs all deploying simultaneously unfurling the sail.

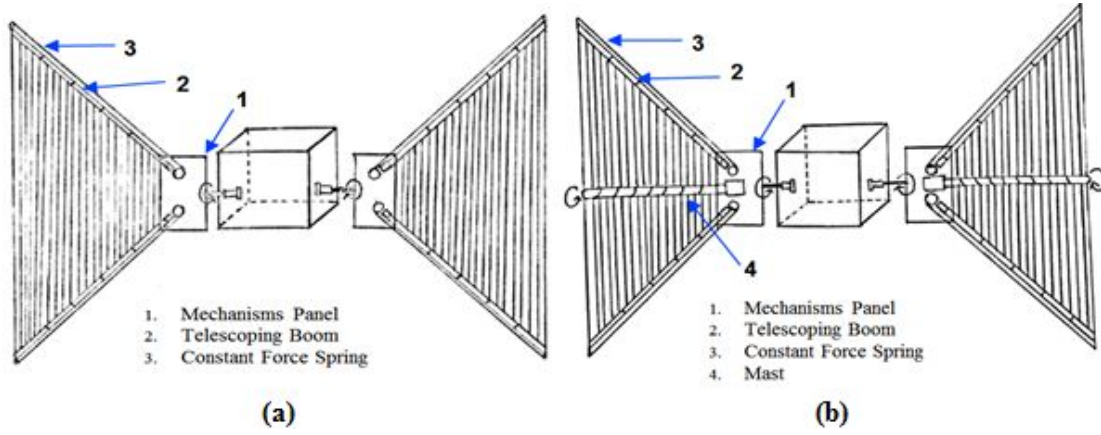


Figure 15. (a) Spacecraft Design Concept 2. **(b)** Spacecraft Design Concept 3 With Mast.

The advantage to this design would be the throttling capability of the mast, therefore changing the sail area which would allow for an increase or decrease in torque, depending on the desired amount. This could also be functional as a collision avoidance maneuver if the threat of ebris is imminent. The challenge of this design would be the manipulation of the mast length while ensuring the sail does not get pinched or tear while winding and unwinding. It was known

that with an arbitrary pressure source, motion of the test article about the z-axis could be created. So began the simulation using a very light movement of air inside of a test chamber. Two paddles hung loosely in the test chamber on a fishing line but it kind of floundered with complete unrepeatable motion. A video of this motion, however, actually became an extremely useful tool in the development of our test setup.

4.3. Testbed Design

4.3.1. Wind Tunnel Test Setup

Attitude control for a solar sail is daunting task that has many obscure challenges just in the simulation alone. Simulations have been performed in testbeds to simulate deployment and stow, checking for repeatability, reliability and accuracy. It was postulated that the tests could be conducted using large mylar sheets laying flat on “air hockey”-like tables, however the velocities from the pressurized air would have to be too great. The resulting high turbulence would cause the sheets to flutter and the data to be lost in this resultant noise. Two paddles constrained to gravity some form of gravity compensating fixture (GCF). The goal of the testbed design is to provide an arbitrary source of pressure that although not scaled to what it would be in space, the very tiny force produced resembles a small enough impulse for a control loop to be designed. These preliminary tests are to be viewed as proof of concepts. The final product delivered is a control loop simulation that demonstrates the feasibility of solar sail attitude control that on the actual spacecraft, translates to using solar wind as its thrust.

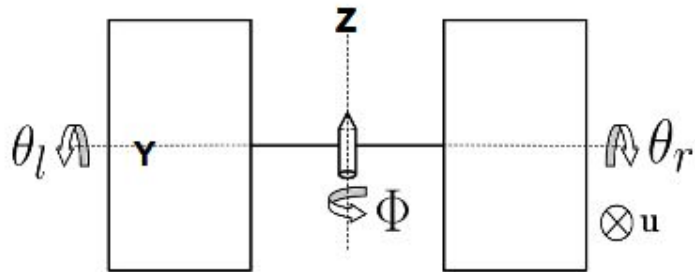


Figure 16. Preliminary Payload Design Concept 1.

The system could still have 1-DOF. However, this notional 3-DOF system was conceived and animated to leap forward and visualize its feasibility seen in Figure 16. It had to be kept in mind that the purpose of the testbed was to demonstrate the feasibility of an attitude control solar sail. Hence, there was a need for a constraint of the test article. The decision was made to restrict its motion about a vertical axis. For the space craft, this would translate to what is known as its “Yaw”, or its torque. Then an open control loop was created to actuate the paddles and counter regulate the test article’s rotation for a desired position output as seen in Figure 18. Later this would mature into a closed loop with the potential for autonomy first using a P controller and then evolving to a PID controller. Given a reference angle and a pressure disturbance changing that angle, it could then correct to the desired final angle. For the space craft, this would translate into its final vector.

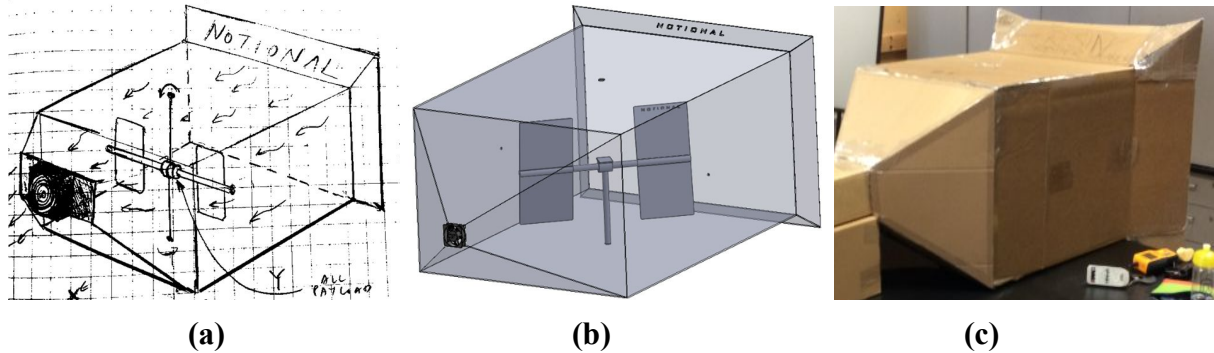


Figure 17. (a) Wind Tunnel Sketch. (b) 3D CAD Model. (c) Preliminary Wind Chamber Build.

Next, the model of the test chamber, Figure 18, was animated and the test article to envision its functionality. Then began the cardboard and duct tape fabrication. It was found right away that there was a need to go from that small CPU fan to a much larger VA industrial air mover to achieve the desired pressure. During the testbed development, it wasn't getting enough thrust on out paddles so the fan size need to be increased. It was quickly determined that a Horizontal Axis Wind Turbines (HAWT) or fans are a poor choice due to their angle of attack fan blade design which do not work for suction. A conventional air mover used for industrial drying applications was procured from Ted Nye, the Senior Design instructor, to record nominal air speeds for suction of over 0.5 m/s or near 1.2 mph which in relative terms, is enough to barely feel on the palm of the hand. This proved to be sufficient for the test.

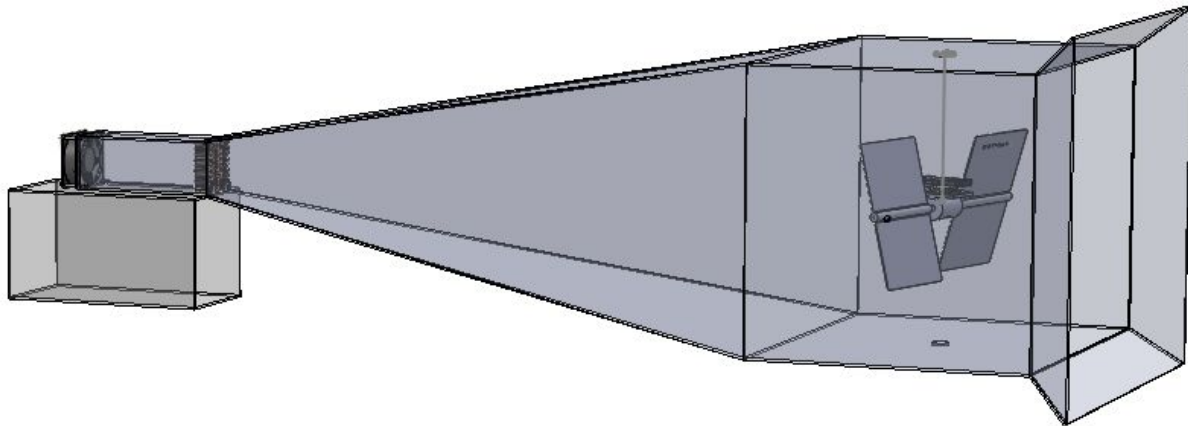


Figure 18. Wind Tunnel Animation.

As with the difficulty of identifying the right type of fan to obtain the low wind velocities desired, the design of the wind tunnel itself was also an arduous process. Each fan had vastly different dimensions and shapes, therefore requiring construction of custom bellmouth shrouds to encompass the entire perimeter. Eventually, a solution was found to connect different shapes as seamlessly as possible and found a way to connect a circular fan diameter to a square throat, which houses the honeycomb screen to promote uniform flow.

4.3.2. Mechanical Design

The first test article, seen in Figure 19, was a quick solution to mitigate manufacturing lead time and prevent any delays of the testing. The goal was to keep it as small and as light as possible. The largest electrical components ended up driving the design such that the minimum size of the footprint would end up becoming 7 cm^3 . A cube platform was coincidentally designed for symmetry and balance as well as its representation of a CubeSat. It was manufactured using a 3D printing additive manufacturing process known as Fused Deposition Modeling (FDM). The printer which extrudes high temperature polymer or plastic like materials was a high end hobby level printer with an open source slicer software capability to process the SolidWorks 3D models as stereolithographic files (STL) to create printable ‘g.’ files. However this version was not very 3D printer friendly on account of the required support material for the cube sides.

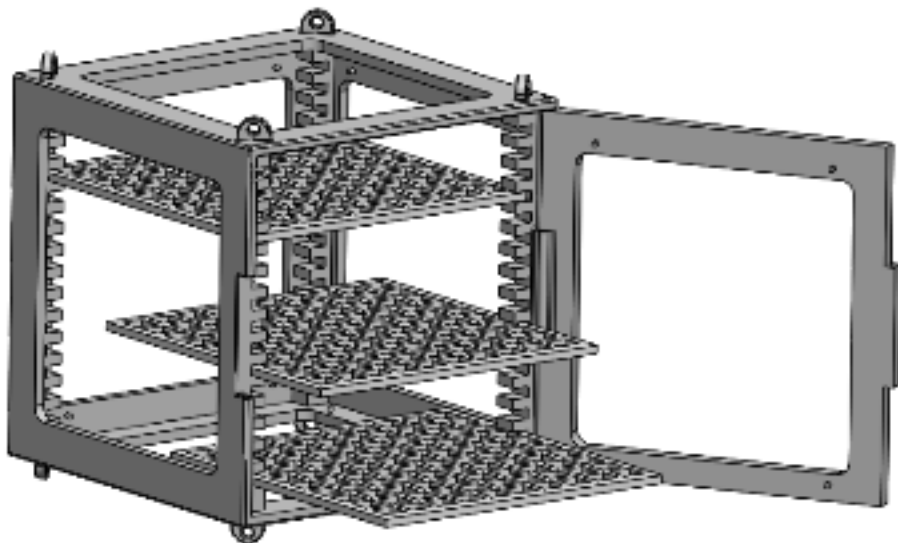


Figure 19. The First 7 cm^3 Test Article Quick Solution

This final version of the test 7 cm^3 cube has a very tight fit with its great fidelity, strength, rigidity and low weight. New print iteration STLs were emailed to Miguel Poly in the CSULA Engineering Senior Design Lab for 3D printing by the Stratasys Uprint 3D printers which had the advantage of dissolvable support material. These prints were useful in the process of assembly and learning what improvements need to be made to meet the requirements of the test. The final models were completed using an Original Prusa i3 MK3 3D printer with a material, according to its Material Safety Data Sheet (MSDS), was very similar to Polylactic Acid (PLA) with a silver metal flake to look like aluminum. The Cube’s redesign was based on a full scale 1U, “Foldable CubeSat” for accessibility while it maintained the relevant shelf positions. A separate flat panel per side improved the 3D print quality because it eliminated the requirement for support any support material. Bearing cups were also added on the top and bottom for the addition of non-lubricated roller thrust bearings.

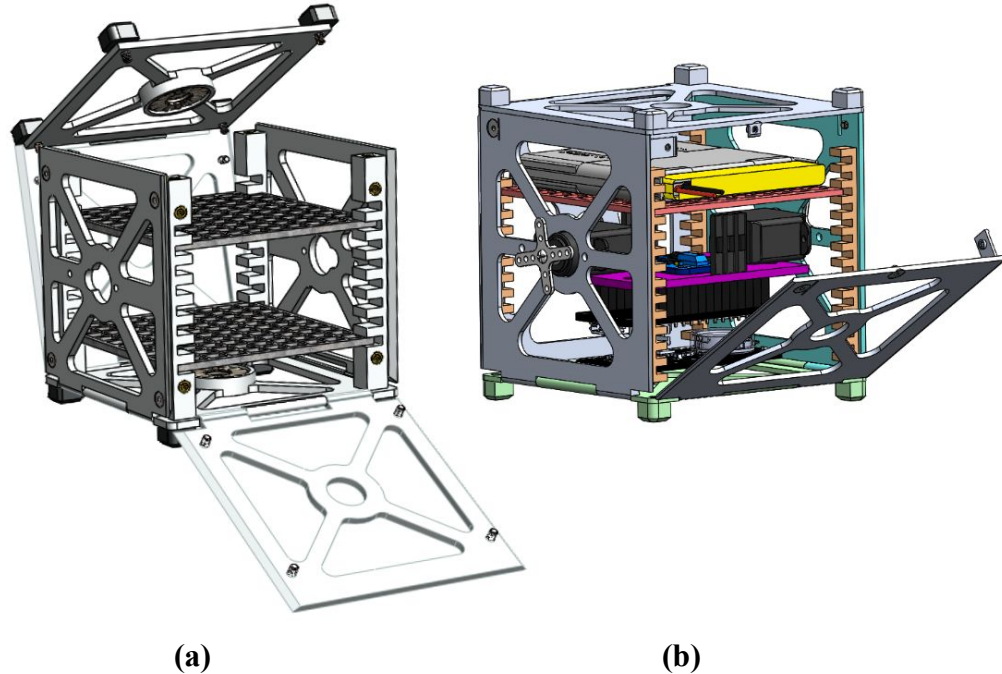


Figure 20. (a) Final Foldable 7cm³ Cube Test Article. **(b)** Test Article with Electronics Stack Up.

Once the Test Article Design for the 3D print model development had been completed, the design for a test article cube design representing the same design approach began. The new cube was dimensioned and tolerated for a machinist to read and produce a CNC machined product from the drawing. This was a basic drawing submission to the CSULA machinery, Blake Cortis. It was quickly learned that the constraints of the CNC machining approach would limit the design to have unhinged flat sides. Water Jetting was not available and CNC Machining was the most cost effective approach. An inexpensive long lasting test article model was produced which will be useful for future teams and their testing. Considerations will need to be made for the aluminium material mass moments of inertia, gravity offloading and perhaps more robust bearings.



Figure 21. (a) CNC Machined 6061 Aluminum Cube (b) Machined Cube Test Article Build

Finally, a bow tie paddle configuration was designed to complement the cross sectional area of the wind tunnel and the extended length of the frame also maximized torque about the YAW (that vertical axis). To keep the paddle frame connected to the servo, the servo fan fitting had to embed into the paddle frame because of the lower fidelity, the 3D printer doesn't print plastic gears well. This new hybrid frame with a lower profile, lighter, carbon fiber hybrid boom reduced vertical stress on the servos to help their lifetime and performance.

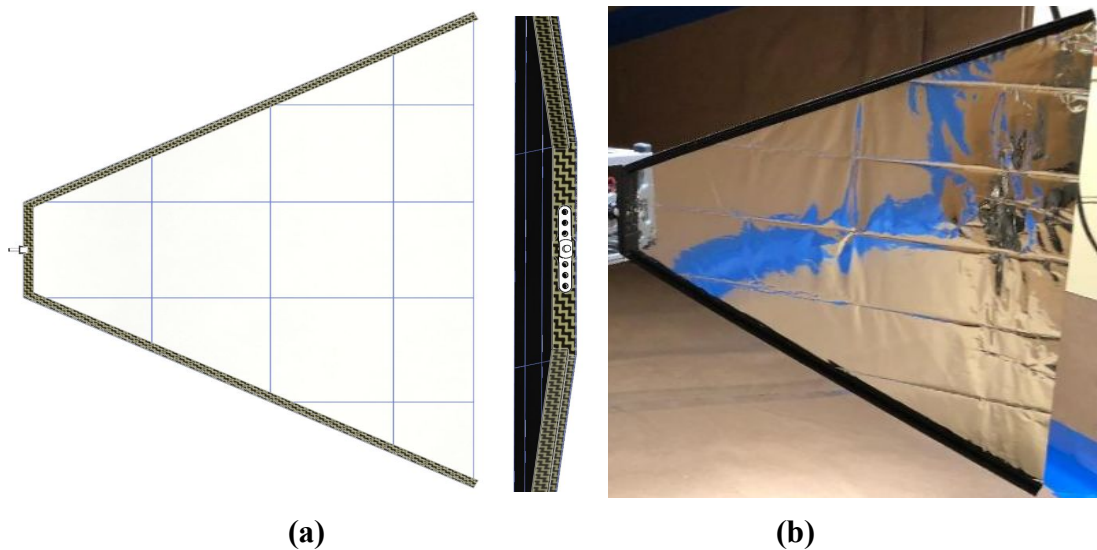


Figure 22. (Left) bow-tie paddle Solidworks mode. (Right) carbon fiber frame with mylar.

The Final Test article was designed and assembled in Solidworks to check form and function, Figure 23a. The Final product was delivered and tested to verify its full functionality and delivery to the senior design expo. All this was the final product delivered, most of the testing was done on an Engineering model created that shared pretty much all of the same requirements. The Test Article was photographed in a photo booth, shown in Figure 23b, to showcase its likeness to the original model.

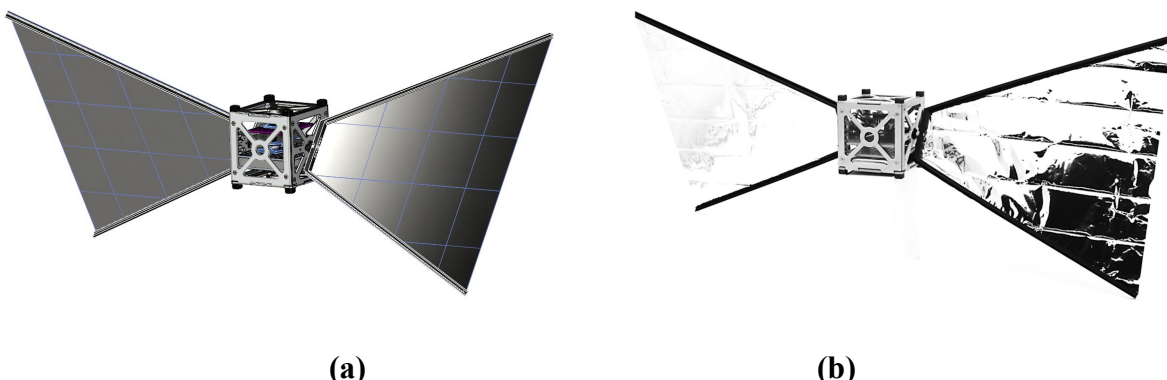


Figure 23. (a) CAD Model (b) Physical Model



Figure 24. Wind Tunnel CAD Model Front Views

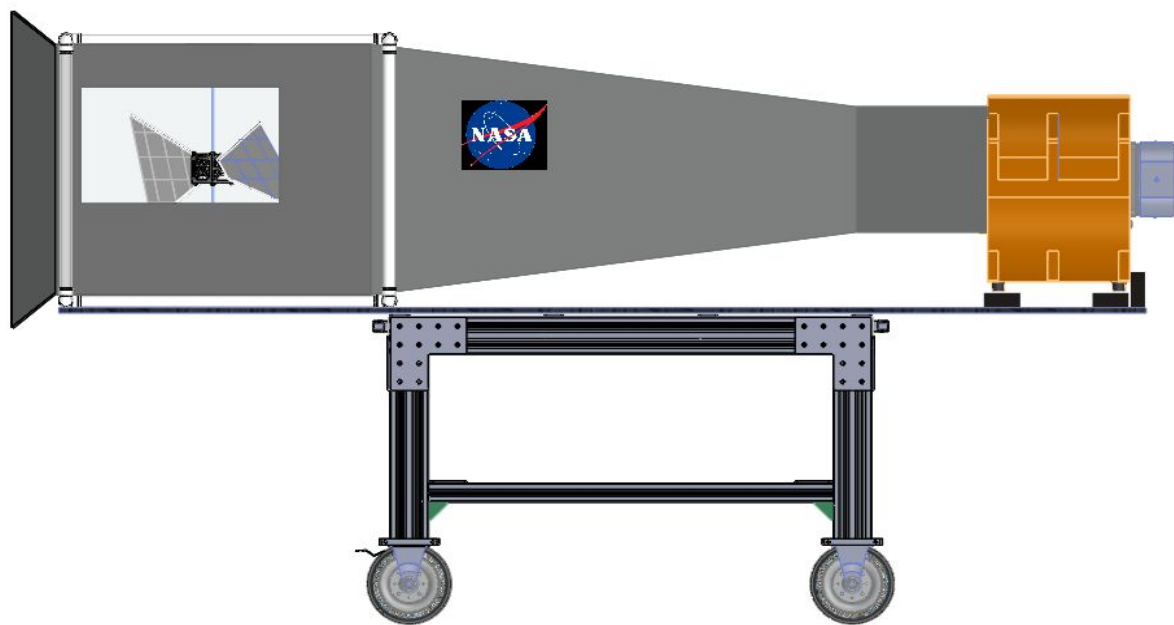


Figure 25. Wind Tunnel CAD Model Side View

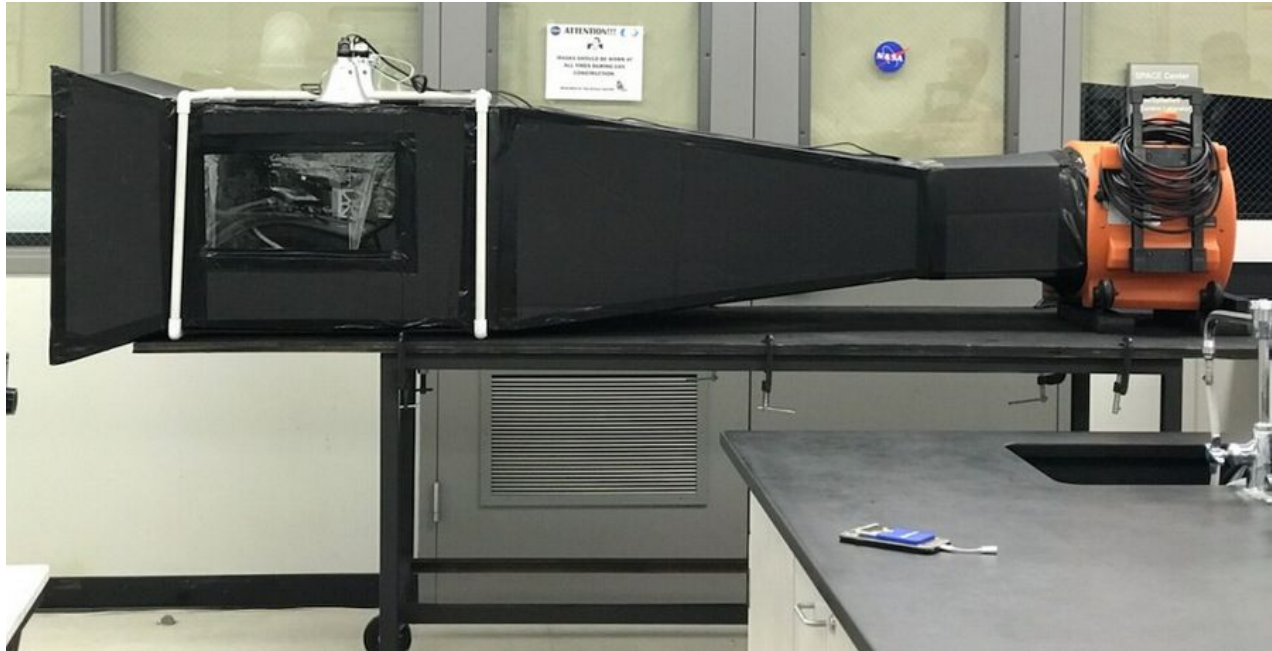


Figure 26. Completed Wind Tunnel

4.3.3. Electrical Design

The electrical design goal of the attitude control system was to incorporate the least amount of components possible, and that those components be of the smallest size possible. The preliminary component stack-up (Figure 27) consisted of a LiPo battery, Bluetooth microcontroller, two servo motors, and an inertial measurement unit sensor (IMU). The power source chosen was a 3.7 V 500 mAh Lithium Ion polymer battery due to its compact size. The capability to connect with the test article wirelessly was paramount, and to achieve this, an Adafruit Feather 32u4 Bluefruit microcontroller was selected. This was on the higher end price-wise but it proved to be the optimal component for the application. It also allowed convenient data acquisition via smartphone when quick tests were necessary. When it came to deciding on a motor to actuate the sail paddles, a Futaba S3114 servo was chosen due to its higher torque (1.7 kg-cm) compared to similar-sized alternatives and compatibility with a closed feedback control loop. Lastly, the IMU chosen was an Adafruit 9-DOF BNO055. Even though only 1 DOF was considered for this project, the higher capabilities of this accelerometer will prove useful when more axes rotations are analyzed down the road.

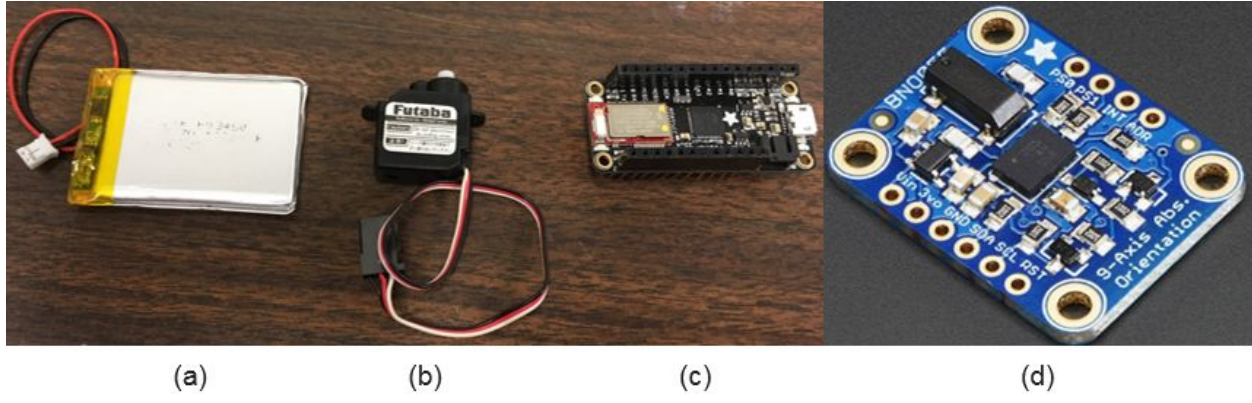


Figure 27. (a) Lipo battery. (b) Servo motor. (c) Bluetooth microcontroller. (d) IMU.

Upon initial breadboard testing, inconsistent data readings were an issue. The issue was narrowed down to the battery being of insufficient power (500 mAh). Once it was replaced by a larger 2500mAh battery, the data became consistent. Once the breadboard testing was finalized, the need for a custom printed circuit board (Figure 28a) became apparent as the desire for quick and easy access to the electronics inside the test article was necessary. Besides routing power from the battery to the IMU and servo motors, this cut down the need for excess wires and connectors. The last component that became valuable was the Adalogger Featherwing to store the data being acquired (Figure 28b). This came equipped with a micro SD card that could be connected to a computer to download large data files. The final component stack-up is shown in Figure 29.

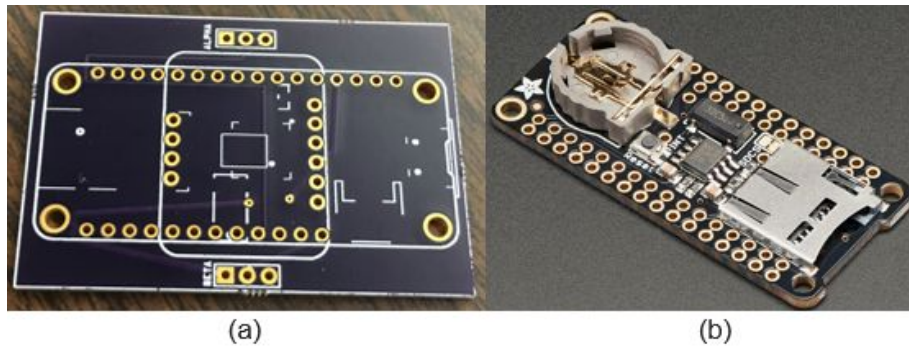


Figure 28. (a) Osh Park Custom Circuit Board. (b) Adalogger Featherwing.

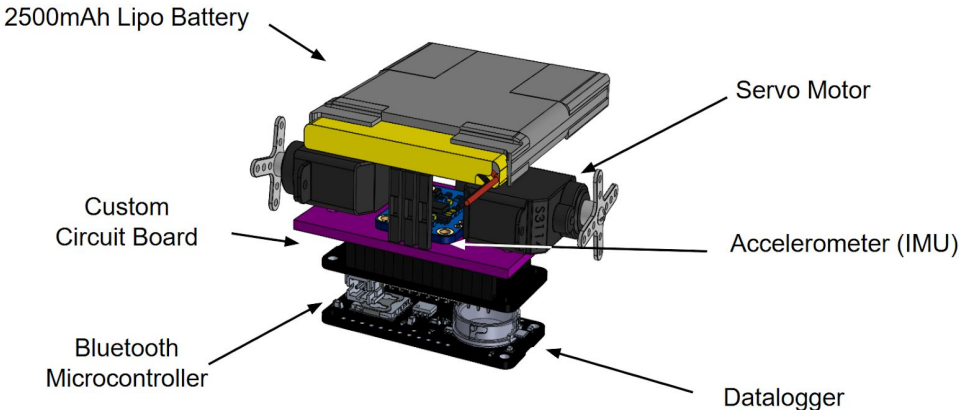


Figure 29. Final Component Stack-up

The block diagram shown in Figure 30 illustrates how the electrical components interface with each other. The battery provides power to the IMU and microcontroller, which then connects and send commands to the two servo motors that control the paddle angles. Data is then sent from the microcontroller to the data logger for storage. The microcontroller was programmed with a closed-loop feedback control algorithm developed in Simulink, with the IMU sensor providing the feedback information as to allow the CubeSat to correct its own orientation and maintain a specified angle as force vectors attempt to rotate it.

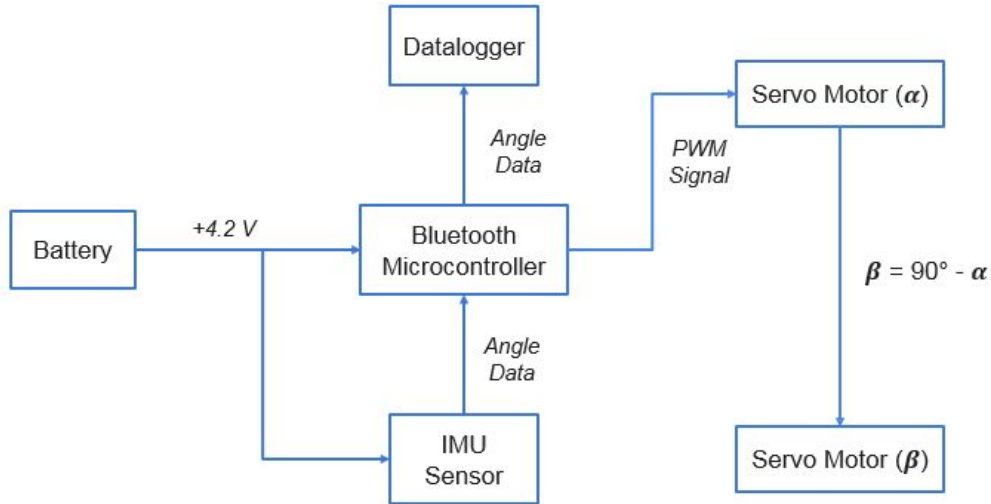


Figure 30. Component Connectivity Block Diagram

4.3.4. Test Integration

Figure 31 shows the completed test article affixed inside the wind tunnel. Custom threaded rods were created to allow for nuts on the bottom side to prevent the test article from coming loose. Roller bearings were placed on top and bottom of the test article frame to allow smooth rotation about z-axis only.



Figure 31. Test Article Setup In Wind Tunnel

5. SIMULATION, TEST, AND RESULTS

5.1. Dynamic Model and Controls Methods

A dynamic model aids in understanding how a closed-loop system and an open-loop system work. A dynamic system's output is measured by a sensor as feedback to a controller and is used to affect change in a system via an actuator.^[7] In order for this system to work, the control system must meet four requirements; tracking, stability, regulation and sensitivity.

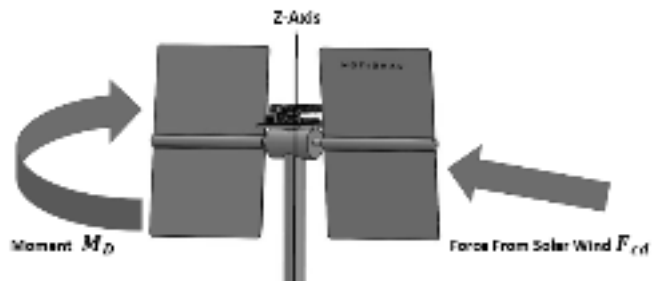


Figure 32. Dynamic Model Testbed

Taking the system as a dynamic system, Newton's Law 2nd law of motion, $\mathbf{F} = \mathbf{ma}$, is applied. The equation of motion (EOM) is derived as follows:

$$F_{cd} + M_D = J\ddot{\theta} \quad (7)$$

$$F_{cd} + M_D = I\dot{s}^2\theta \quad (8)$$

$$U = I\dot{s}^2\theta \quad (9)$$

Once the values are achieved the next step is to find the transfer function of the system. The Transfer function then becomes:

$$\frac{\theta}{U} = \frac{1}{J\dot{s}^2} \quad (10)$$

Stability prevents the the system from a situation that would send the loop to infinity or diverge so that the target output will never be reached. When tracking is involved, this shows that the system's output should track the commands reference signal as closely as possible. Tracking is used to determine the steady state error of in output signal of the dynamic model behaviour as well as the stability of the plant. Tuning of the system is required in order to make sure that this system works in a real world scenario. Improper tuning will result in a system that is too sensitive. For this 1 DOF preliminary testbed model (Figure 33), a PID controller was implemented and angle-keeping was achieved at low wind speeds. More tuning is required to refine the rise time, settling time and overshoot of the system^[7].

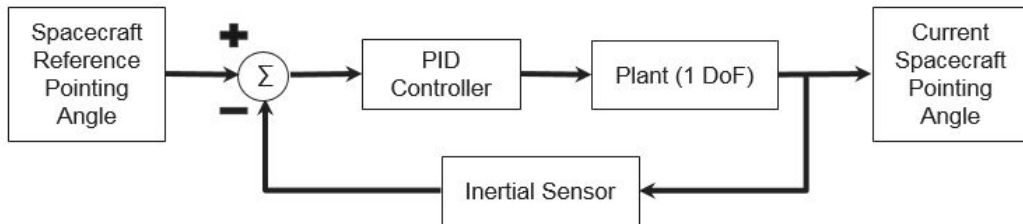


Figure 33. Closed Feedback Control System Loop.

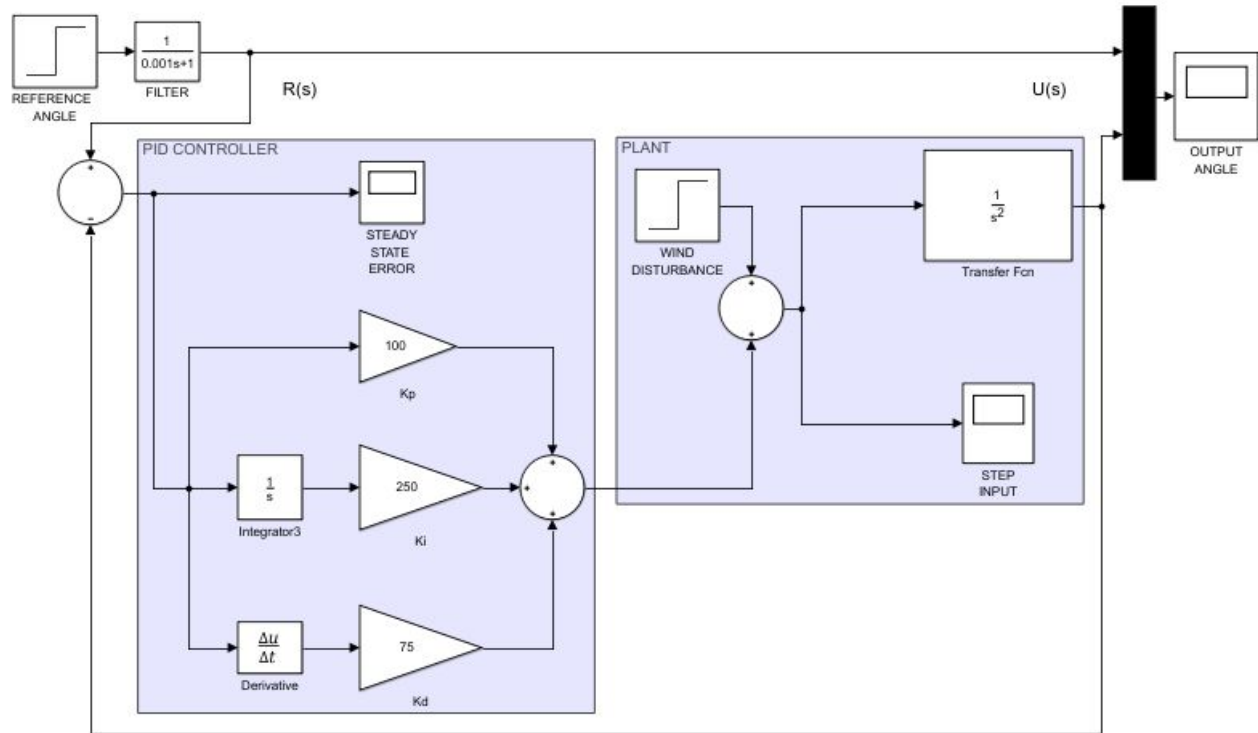


Figure 34. Simulink Control Model for 1 DOF Testbed.

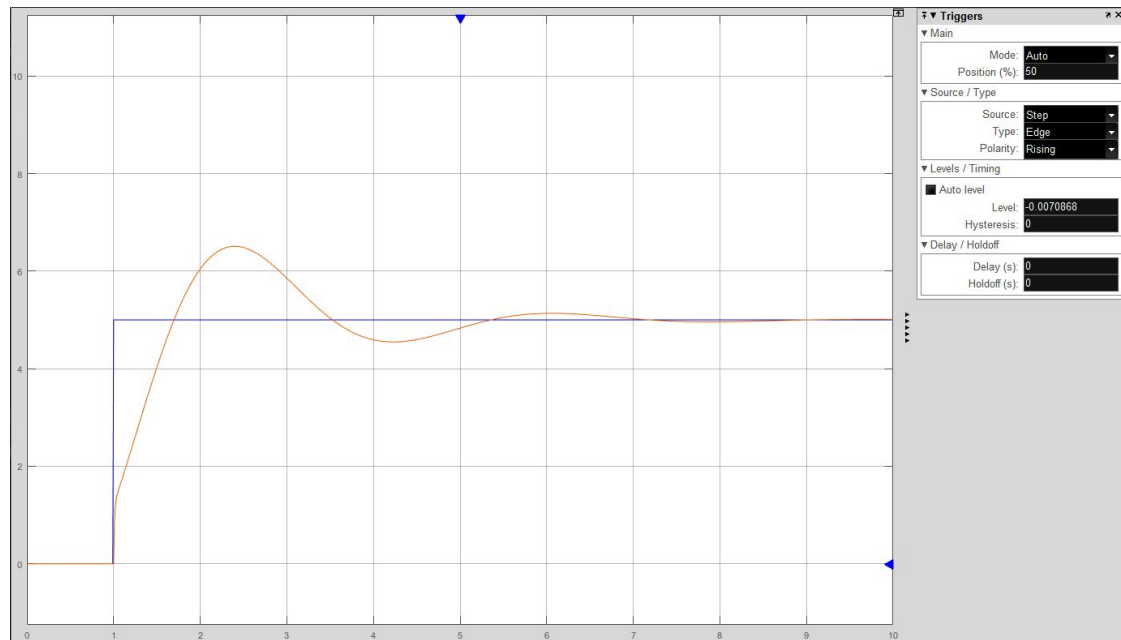


Figure 35. A notional PID controller for a 1 DOF testbed.

5.1.1. Control Dynamics of a Single Paddle Setup

The first iteration of the test article will sit atop a narrow spindle and consist of a single aluminized mylar paddle with a counterweight at the other end. This test article consists of a balanced mass containing one RC servo to control the paddle; and an RF transmitter, inertial measurement unit (IMU), Arduino Micro microcontroller, and Bluetooth transmitter to send commands to the unit wirelessly.

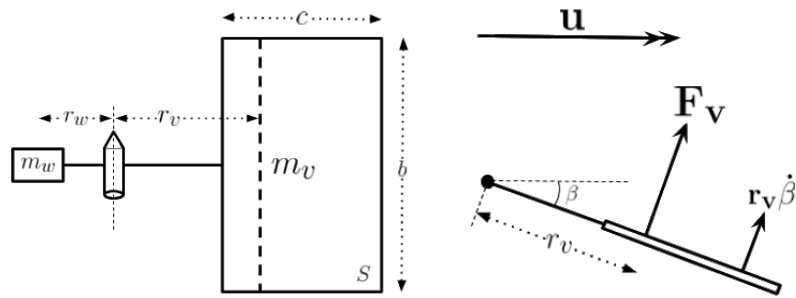


Figure 36. Single Paddle Set-Up and Force Vectors.

$$\tau = \frac{r_v F_v}{\beta} \quad (6)$$

As force F_v is exerted on the paddle surface, the angle of incidence β will change, resulting in supplementary force vector $r_v \dot{\beta}$, where $\dot{\beta}$ is angular velocity, expressed in Newtonian notation. The mathematics may be further developed to obtain the equilibrium condition, or steady state of the single vane system. Considering moment of inertia I , steady state is achieved under the following condition:

$$-I \ddot{\beta} = \tau \beta + \left(\frac{r_v \tau}{u} \right) \beta \quad (7)$$

F_v is the vector projection of the force due to u along the direction of rotation. A Simulink model incorporating this mathematics has not yet been implemented.

5.1.2 Control Dynamics of a Double Paddle Setup

To perform basic angle-keeping functions, a way to mitigate the positive angular deflection of the test article (assuming counter-clockwise rotation is taken to be positive) must be implemented. To do this, a double paddle apparatus will be created with independently movable vanes.

The control dynamics of this setup are identical to that above, except that there is a force created by the left-side paddle that directly opposes the motion of the right-side paddle. The closed-loop control models for both the above setups have not yet been developed. The next section details an open-loop control model implemented on Simulink for the double paddle setup.

To evaluate the feasibility of solar steering due to mechanical actuation, a Simulink graphical user interface (GUI) was implemented. This tool outputs angular acceleration, velocity, and position given the pitch angles of two solar sail paddles. The model considers a perfectly reflective, ideal, square solar sail with side length s . It then splits this square into two independently movable portions called “vanes” that, when rotated, produce a net torque about the center of mass of the spacecraft.

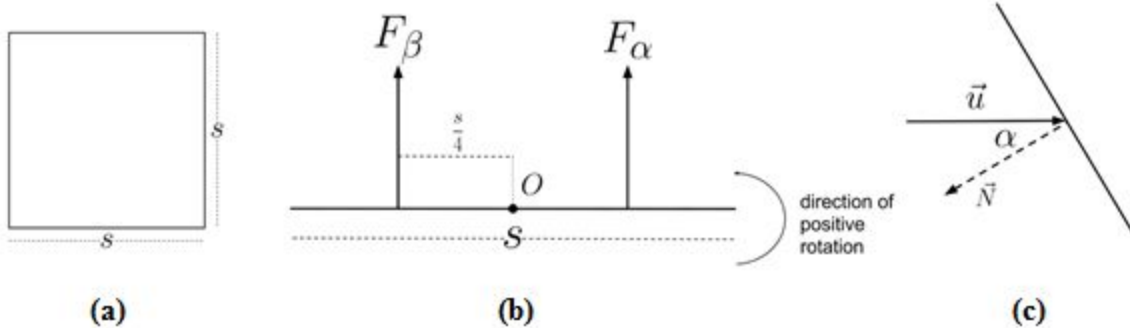


Figure 37. (a) Ideal solar sail with perfect reflectivity and side length s . (b) Side view of (a) showing a difference in force generated by altering the pitch angle of each “paddle” to different values; a net torque will be generated about O as a result of this difference in forces. (c) Side view of one of the paddles, where N is the vector normal to the solar sail surface, and u is the solar radiation vector.

5.2. Simulink Methodology

5.2.1 Calculations for the Mechanical Actuation Steering Method

First, Eq. (8) to calculate pressure due to solar radiation for a perfectly reflective planar surface was considered:

$$P_{reflect} = \frac{2W}{cR^2} \cos^2 \alpha \quad (8)$$

where W is the solar irradiance constant ($W = 1361 \text{ W/m}^2$ at 1 AU from the sun), c is the speed of light, R is the distance of the solar sail from the sun in astronomical units (AU), and α is the angle between the normal vector to the surface and the angle of incidence of the incoming light ray (Figure #c). This formula may be used to find the torque about point O (Figure 1B). Torque was calculated using Eq. (9):

$$\tau = Fl = PAI \quad (9)$$

where $A = \frac{1}{2}s^2$ and $l = \frac{1}{4}s$.

The torque with respect to point O for each paddle may be calculated using (2). A MATLAB function to calculate torque assuming perfect reflectivity is shown here:

```

function torque = solarsail_torque(W, c, R, side, angle)
P = (2*W/(c*R^2))*(cosd(angle))^2;
A = 0.5*(side^2);
l = 0.25*side;

torque = P*A*l;

```

Taking counterclockwise rotation as positive, the net torque about point O may be found employing Eq. (10):

$$\tau_O = \tau_\alpha - \tau_\beta \quad (10)$$

The moment of inertia (11) was found using the following formula for moment of inertia of a square plane:

$$I = \frac{s^4}{12} \quad (11)$$

The angular acceleration (12) was calculated using the following relation:

$$\ddot{\theta} = \frac{\tau}{I} \quad (12)$$

5.2.2 Calculations for the Reflectivity Change Steering Method

A similar procedure was used to create the a Simulink block diagram to model angular response for a reflectivity change steering method. This subsystem outputs angle responses given the “best case scenario” torque for the system. The “best-case scenario” is defined under the following three conditions:

1. Considers perfectly reflective, ideal planar surface for exactly one-half of the solar sail area
2. Considers perfectly absorptive, ideal planar surface for exactly one-half of the solar sail area
3. Assumes perfect orthogonality to incoming sun vector (constant angle = 0°)

The torque for the reflective half of the solar sail was be found by considering equations (9) and (10), and setting $\alpha = 0^\circ$. The torque for the absorptive half of the solar sail was be found by considering Eq. (13) for solar radiation pressure due to a perfectly absorptive surface:

$$P_{absorb} = \frac{1}{2}P_{reflect} = \frac{W}{cR^2} \cos^2 \alpha \quad (13)$$

The pressure due to perfect reflection and that due to perfect absorption (13) may be used to find the magnitude of the force vectors for each half of the solar sail, which can then be used to find each torque. A MATLAB function to calculate torque assuming perfect absorptivity is shown here:

```

function torque = solarsail_torque_absorptive(W, c, R, side, angle)
P = (W/(c*R^2))*(cosd(angle))^2;
A = 0.5*(side^2);

```

```

l = 0.25*side;
torque = P*A*l;

```

The torque due to absorption may then be subtracted from the torque due to reflection to find net torque about point O , as shown below:

$$\tau_O = \tau_{reflect} - \tau_{absorb} \quad (14)$$

As in the previous section, the angular acceleration may be found using Eq. (12).

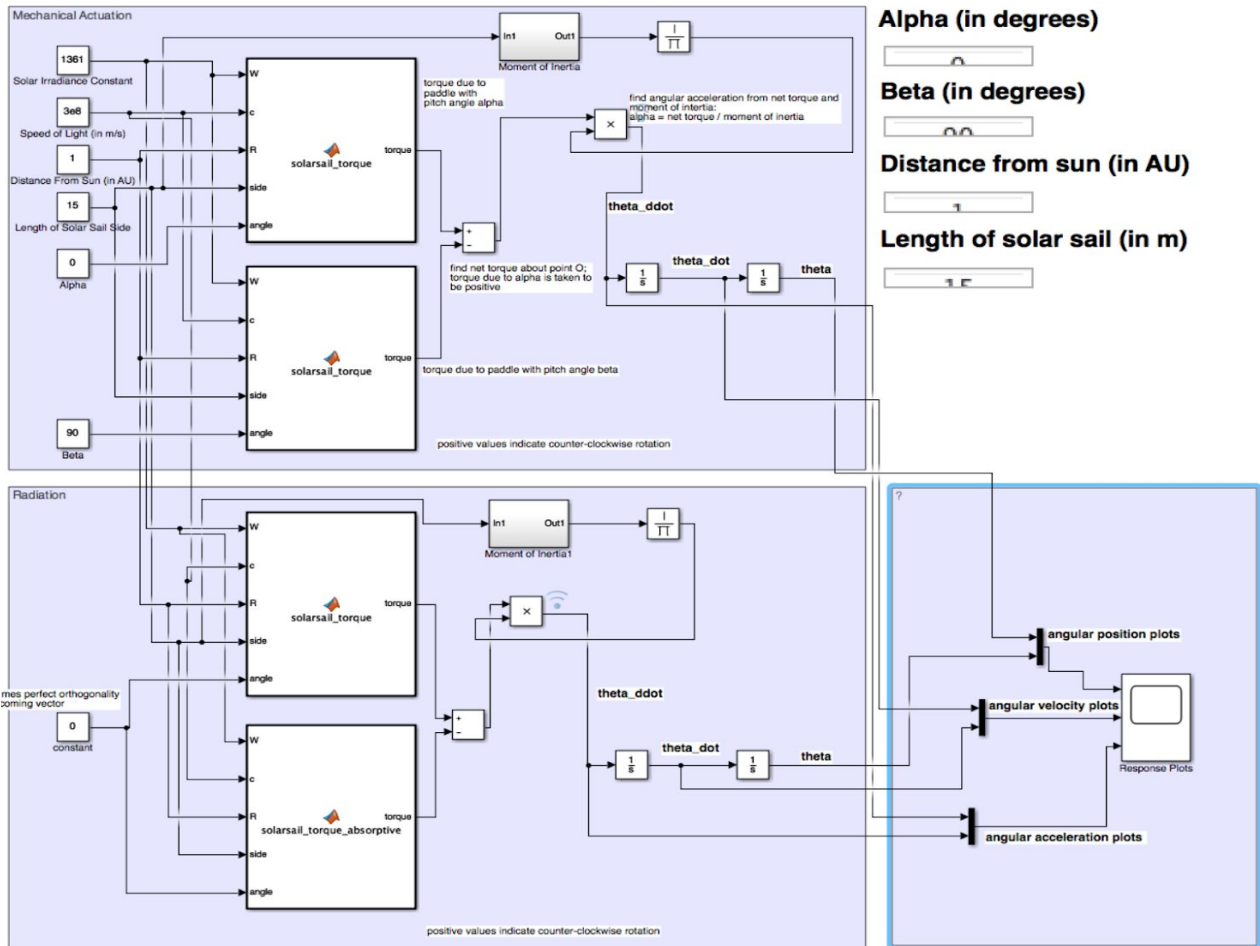


Figure 38. Simulink Solar Sail Angular Acceleration Calculator.

5.2.3. Preliminary Results

The preliminary simulation output results greatly support the project thesis. The angular acceleration plots (Figure 39) show that the mechanical actuation steering method achieves approximately twice as fast angular acceleration than the reflectivity change steering method. Considering this faster method, the angular position plot shows that the apparatus is able to achieve a one-degree differential in thirty minutes. It should be noted that these results are notional, as a massless plane with a square area is being considered, and perfect reflectivity is

assumed. In real life, the efficiency of a solar sail varies from $0.75 < \eta < 0.92$, yielding much smaller magnitudes than those in the plots shown here.

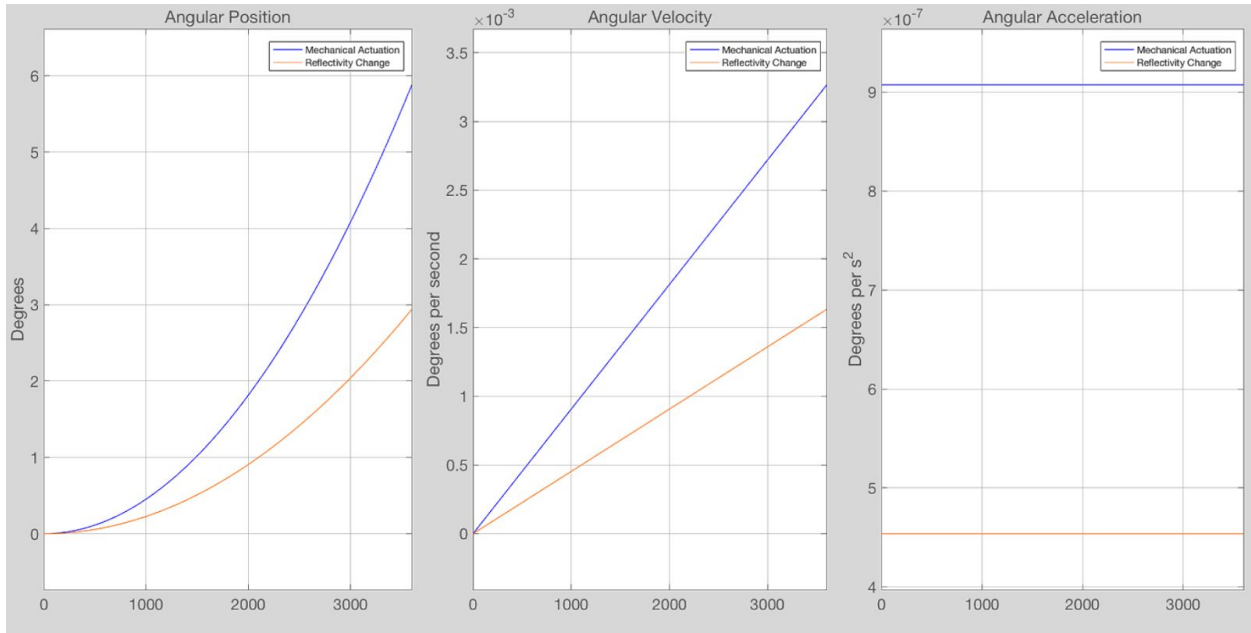


Figure 39. Mechanical Actuation vs. Reflectivity Change Plots.

5.3. Computational Fluid Dynamics Model

5.3.1. Flow Simulation Settings

Flow simulations is the bridge between the Simulink and wind tunnel testing. Simulations will reveal the percent differences between force and torques achieve during simulations; this will validate the feasibility of using a wind tunnel to simulate solar sail behavior in space. Solidworks flow simulations will consider area, A ; air density, ρ ; velocity, v ; and drag coefficient, C_D to calculate drag force, F_D . Force due to drag is used to compare the force due to solar radiation pressure. Area of sails will be equal to area used in the Simulink model. Density used for air was $1.20 \frac{kg}{m^3}$. Drag coefficient of a flat plate is around 1.04; this drag coefficient was used to determine the necessary velocity to obtain equal to similar forces obtained through Simulink model. Drag force was obtained through Equation 6 where everything is known except the velocity required to obtain drag force. Table 10 displays the flow simulations settings for all testing done through SolidWorks.

Table 10. Flow Settings

Settings	Specification
Analysis Type	External Flow
Reference Axis	Z-axis
Fluid	Air
Flow Type	Laminar
Pressure	101325 Pa
Temperature	293 K
Velocity	0.003814614 m/s
Fluid Density	1.20 kg/m ³

5.3.2. Flow Simulation Paddle Angles and Mesh

Flow simulations were conducted with various angles needed to adjust satellite attitude. Angles like alpha at 0 beta at 90, alpha at 30 beta at 60, alpha at 45 beta at 45 and alpha 60 beta 30 were prioritized and recorded. Paddles with larger difference in angles should create larger torques; paddles with minimal degree difference will theoretically generate small torques. Local mesh was generated where level of fluid cell refinement was set at level 4. Advance refinement was used where small solid feature refinement, curvature and tolerance levels were set at level 2.

5.3.3. Flow Simulation Goals

Flow simulation goals were to obtain normal forces achieved on both frontal and rear of alpha and beta paddles. The difference in forces will create a net torque that will help turn the satellite. Table 11 and 12 displays the normal forces on both front and rear surface.

Table 11. Surface Goal Alpha Paddle

Type	Surface Goal
Goal type	Normal Force
Faces	Alpha Paddle Front Alpha Paddle Rear
Coordinate system	Global coordinate system
Use in convergence	On

Table 12. Surface Goal Beta Paddle

Type	Surface Goal
Goal type	Normal Force
Faces	Beta Paddle Front Beta Paddle Rear
Coordinate system	Global coordinate system
Use in convergence	On

5.3.4. Flow Simulation Equation Goals

Solidworks was provided with formulas that would provide net torques created by flow simulations where moment arm was set at 2.84 meters. Equations will take surface goal achieved normal forces to provide net torques similar to Simulink method. Where rear and frontal forces on individual paddles were added and then multiplied by moment arm. The difference obtain when subtracting paddles achieved result in a net torque. Figure 40 shows a flow simulation of air displaying the flow trajectory and surface plot of relative pressure.

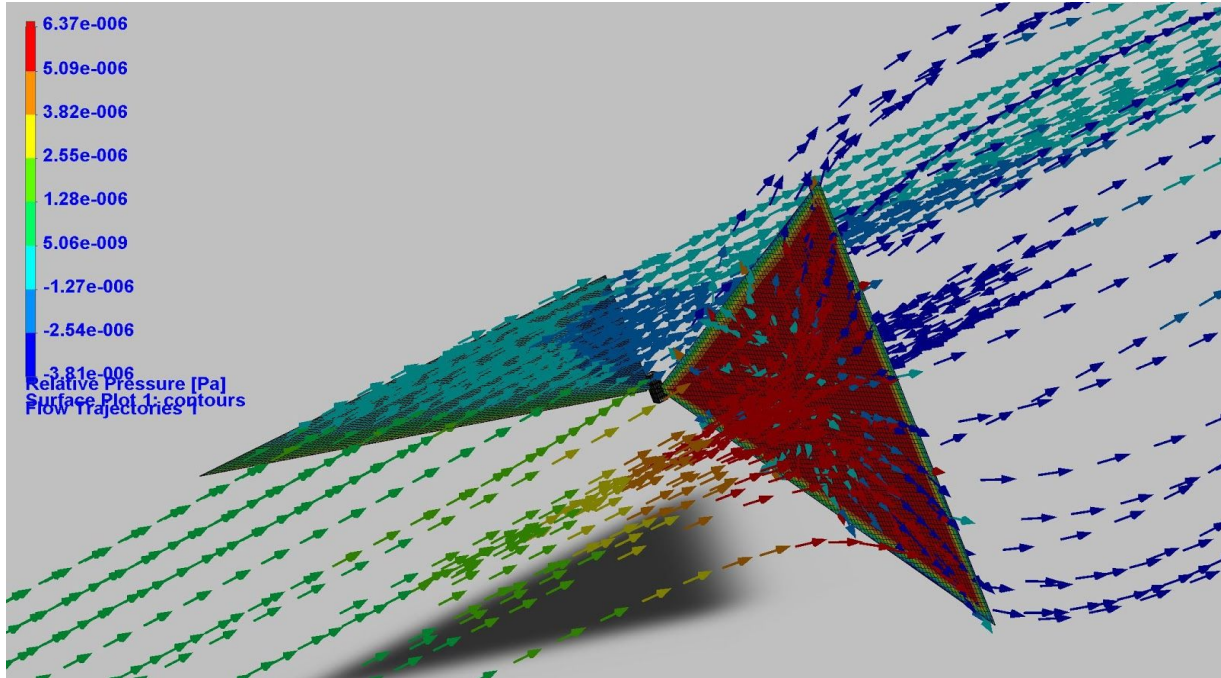


Figure 40. Solidworks CFD Simulation

Figure 41 and 42 represent both the forces and torques obtained from simulations of alpha paddle at 0 and beta at 90 degrees; Table 13 reflect average results.

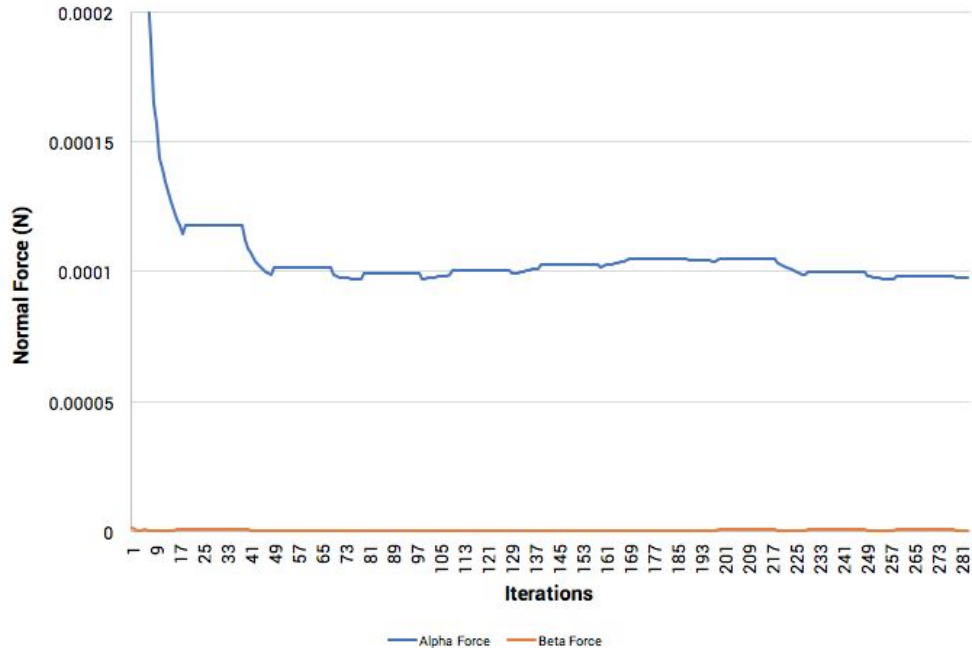
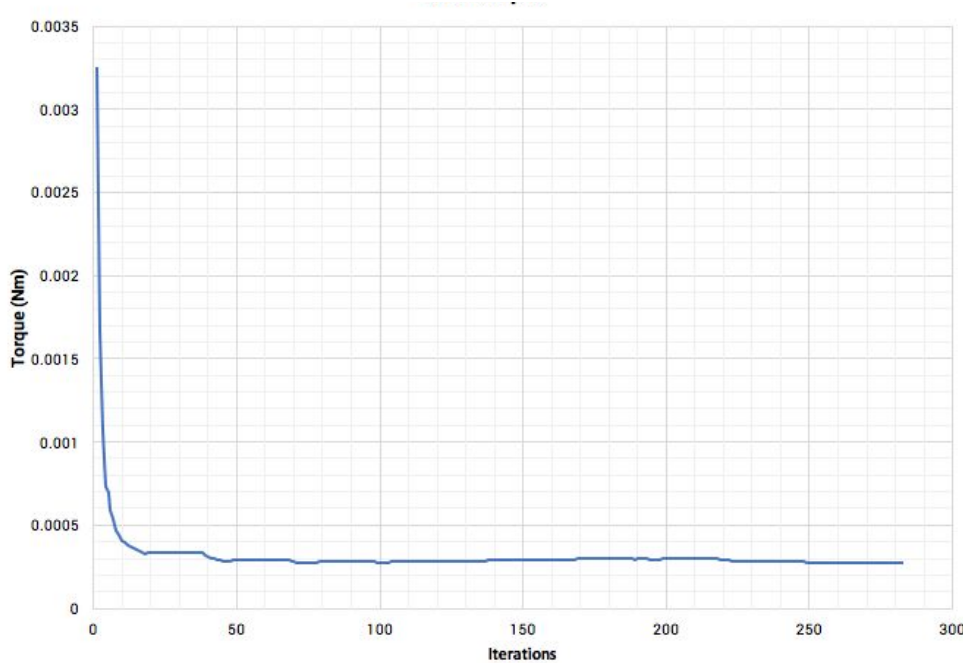


Figure 41. Normal Force Fluid Simulation

**Figure 42.** Net Torque**Table 13.** Average Forces and Torque

Goal Name	Averaged Value	Minimum Value	Maximum Value
Alpha Force	9.80201E-05	9.71726E-05	9.97079E-05
Beta Force	5.25061E-07	3.99358E-07	6.02552E-07
Net Torque	0.000276886	0.000274738	0.00028156

Figure 43 shows the flow trajectory and surface plot of alpha paddle at 30° , beta at 60° .

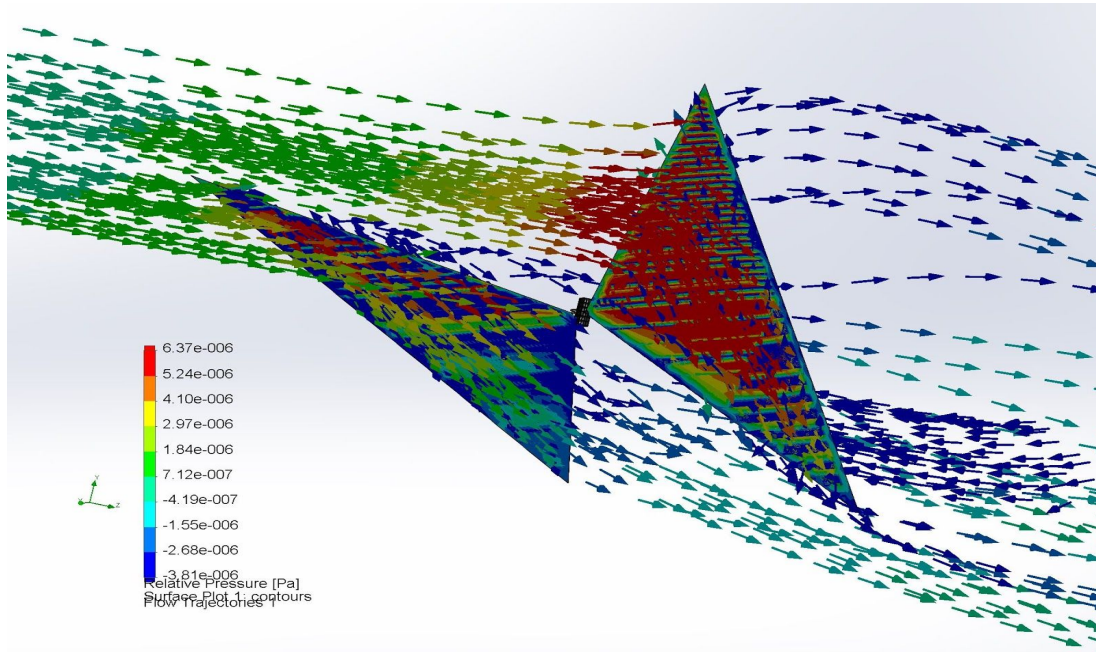


Figure 43. Flow Trajectory Alpha 30°, Beta 60°

Figures 44 and 45 are the resulting graphs from flow simulations from Alpha 30°, Beta 60°.

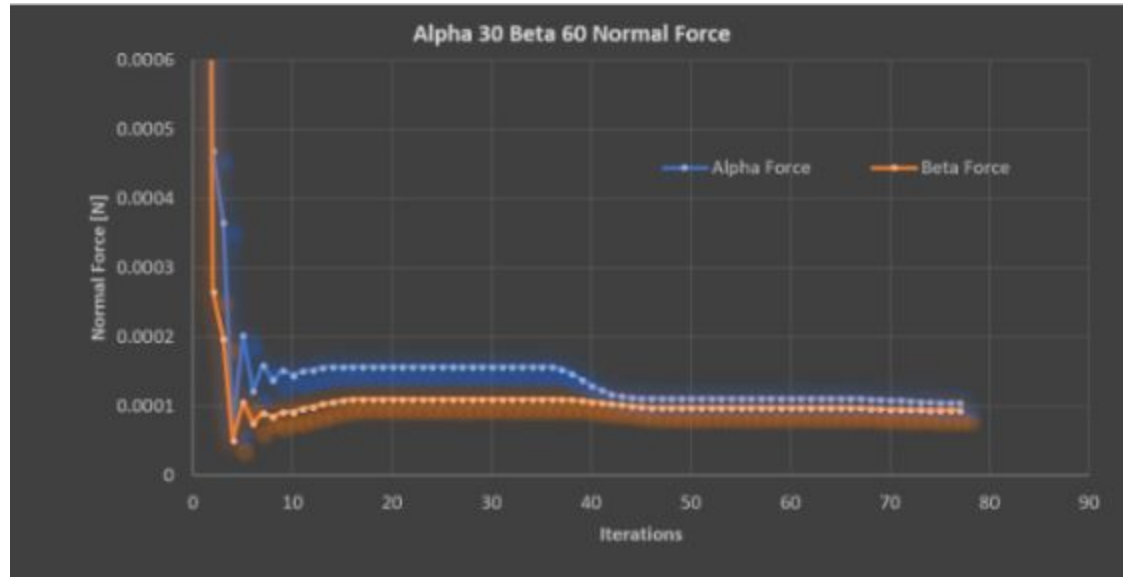


Figure 44. Alpha 30°, Beta 60° Normal Force

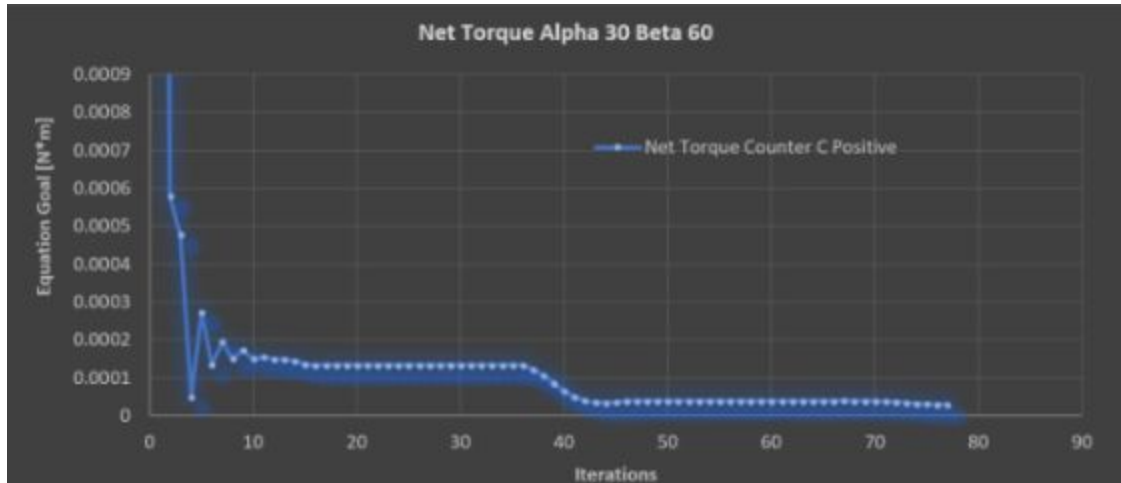
**Figure 45.** Net Torque Alpha 30°, Beta 60°

Table 14 reflects the average value, min value and maximum value obtained by flow simulations of Alpha 30°, Beta 60°.

Table 14. Flow Simulations of Alpha 30°, Beta 60°

Goal Name	Averaged Value	Minimum Value	Maximum Value
Alpha Force	0.000110714	0.000105119	0.000112132
Beta Force	9.74524E-05	9.44208E-05	9.84902E-05
Net Torque Counter C Positive	3.76627E-05	3.01917E-05	4.02243E-05

The flow simulations are all almost equal to Simulink model with the exception of alpha paddle at 45, beta paddle at 45. These simulations due to fluid behavior naturally create some sort of minuscule torque as shown in Figures 46 and 47.

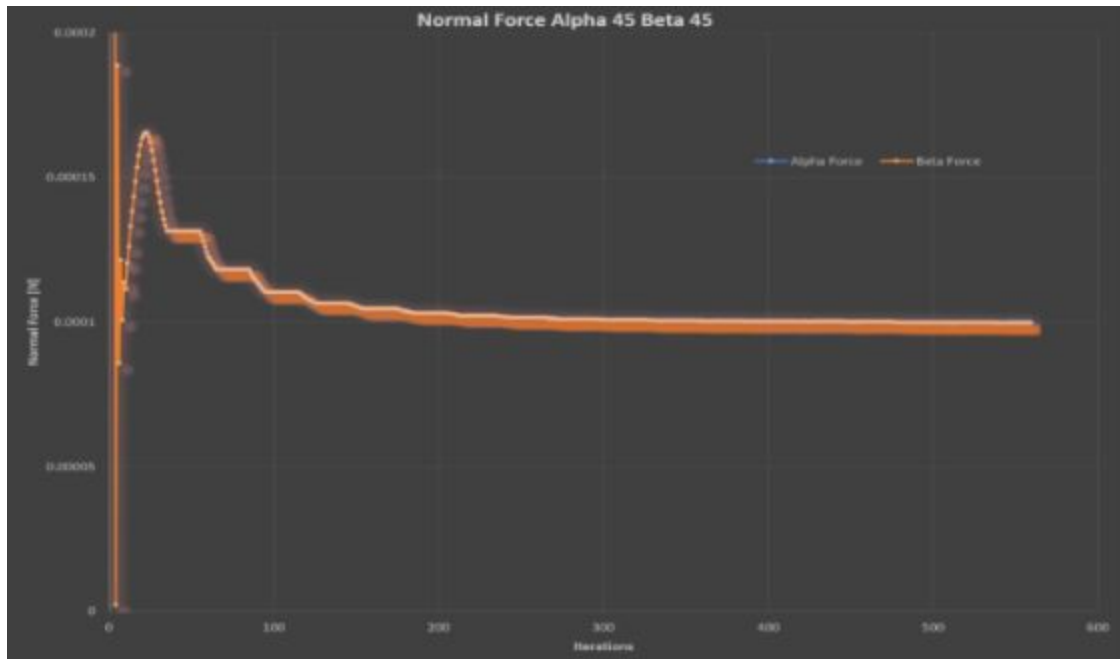


Figure 46. Normal Force Alpha 45°, Beta 45°

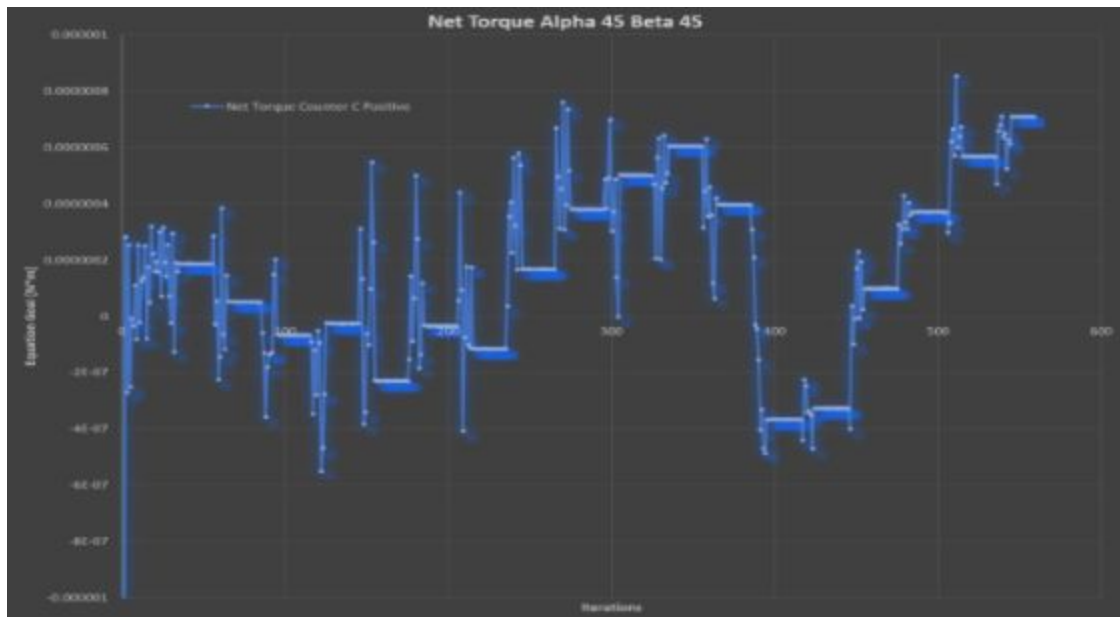


Figure 47. Net Torque Alpha 45°, Beta 45°

5.3.5. Flow Simulation vs. Simulink

Comparing Simulink results, what the solar sails would experience in space to Solidworks Flow simulations, what the solar sails would experience in a wind tunnel; return with minuscule differences. Table 15 displays the difference in angles ranging from 0 to 90. Percent difference was most close when paddles were either streamline to fluid flow or perpendicular to it. Percent differences changed when paddles were at or around 30 to 60 degree range; this is due to the change in drag coefficient when the paddles aren't perpendicular to fluid flow. The highest percent difference was 3.96%; validating the use of a wind tunnel for simulations is helpful to obtain similar torques as solar sails would experience in space.

Table 15. Simulink vs. CFD Simulations

Angles (Alpha - Beta)		Net Torque Simulink	Net Torque CFD Simulation	% Difference
0°	90°	276 μNm	276.8 μNm	0.30%
30°	60°	36.9 μNm	37.66 μNm	2.04%
60°	30°	-36.9 μNm	-38.39 μNm	3.96%

5.4. Test Data

5.4.1. Open Loop Controller Data

An open loop controller was developed to be able to test how the test article behaved in the wind tunnel when the solar paddles were in certain angle configurations. With the open loop controller, the alpha paddle angle with respect to the wind flow is able to change. When the alpha paddle angle was changed, the beta paddle angle was automatically changed to the difference of the alpha paddle angle and 90 degrees. Using this controller, plotting three different paddle angle configurations can be achieved, one where the alpha paddle is at 0 degrees, and the beta paddle is at 90 degrees; another where the alpha paddle is at 90 degrees, and the beta paddle is at 0 degrees and the last one, where both the alpha and beta paddles are at 45 degrees.

The tested paddle angle configuration was tested when the alpha paddle angle was at 0 degrees, and the beta paddle angle was at 90 degrees. Commanding the test article to stay facing at 270 degrees, which is the face of the test article is parallel to the wind vector. However, in this configuration, see Figure 48, it shows there was a lot of jitter happening with the test article in the wind tunnel. The test article was hovering between 260 and 282 degrees, which shows

promising results because the test article can at least point in the correct direction with minimal deviation but minimizing as much as jitter is preferred.

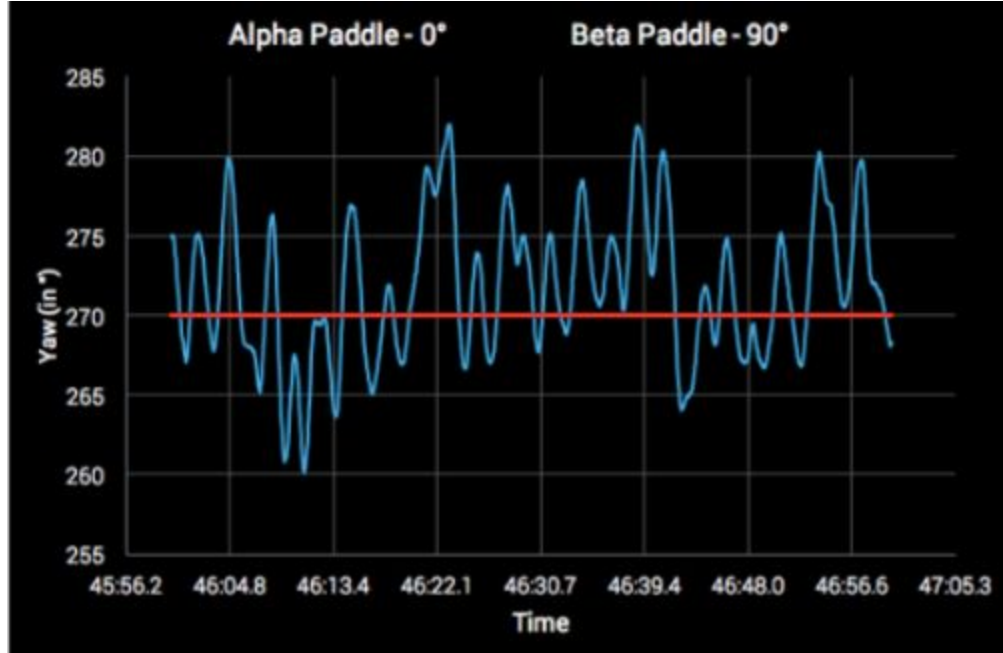


Figure 48. Test Results of Alpha 0°, Beta 90°

The second paddle angle configuration was tested when the alpha paddle angle was at 90 degrees, and the beta paddle angle was at 0 degrees. If commanding the test article to stay facing 90 degrees, which the face of the test article is parallel to the wind vector but is facing the opposite direction as when the alpha paddle is at 0 degrees, and beta paddle is at 90 degrees. In this configuration, seen in Figure 49, the test article in the wind tunnel was jittering. The test article was hovering between 82 and 104 degrees which again shows promising results because the test article can point in the correct direction, but the jitter is still apparent, and the need to develop different solutions to counteract this jitter is necessary.

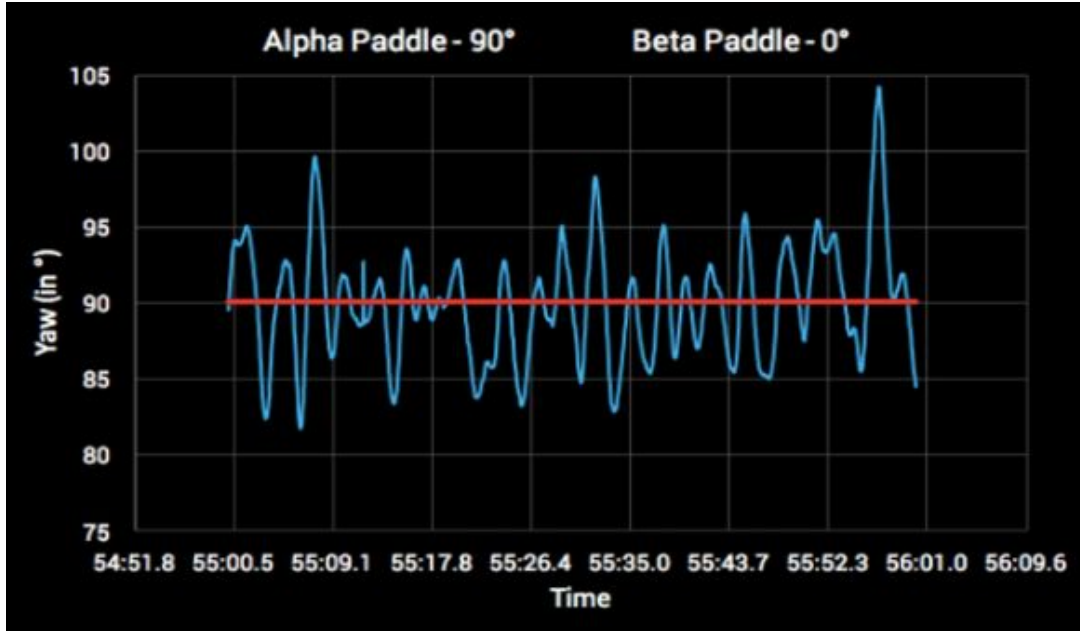


Figure 49. Test Results of Alpha 90°, Beta 0°

The last paddle angle configuration that tested was when the alpha paddle angle and the beta paddle angle were both at 45 degrees, this configuration allows equal amount of area on the both paddles to be facing the wind. In this configuration, if commanding the test article to be facing 180 degrees, which the face of the test article was perpendicular to the wind vector, but seen in Figure 50, the jitter was still apparent. While in this configuration, the jitter compromised the results, and the desired output of 180 degrees was achieved on a minimal basis. From Figure 3, it seemed the results were elevated on the graph and shows a center point of about 195 degrees, which is not preferred.

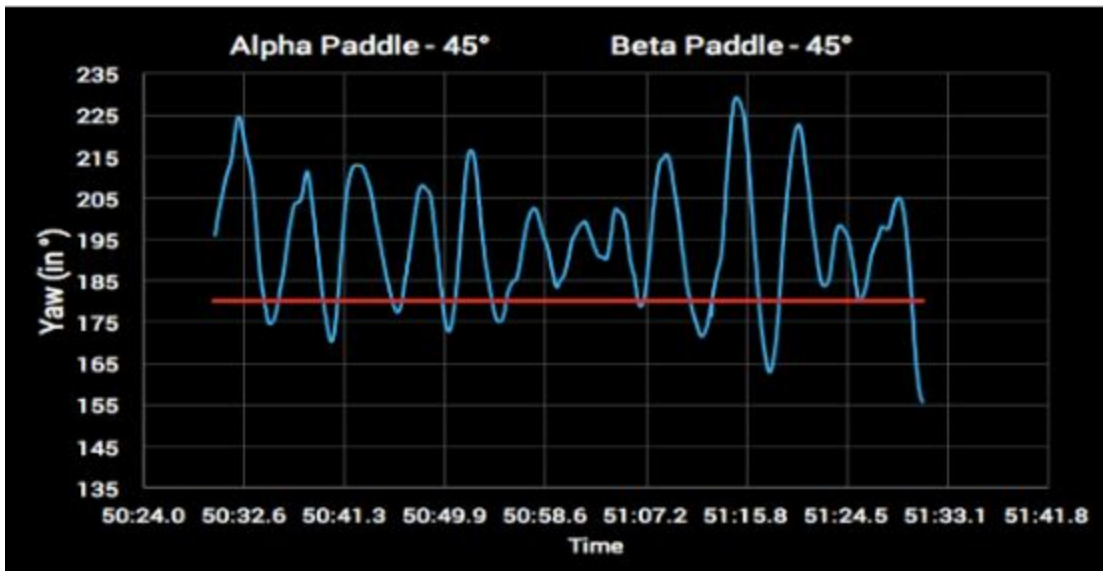


Figure 50. Test Results of Alpha 45°, Beta 45°

5.4.2. PID Controller

In order to reduce the jitter that was seen throughout the wind tunnel testing, where can be seen in the previous graphs, a PID controller was implemented. Using a PID controller also allows to automate angle correction of the test article. The difficulty in implementing this PID controller was tuning the PID controller with the correct proportional, derivative, and integral constants. At first, a brute force method required iterating through each combination of constants, but that was time consuming. Therefore, the PID tuner app in MATLAB is used to find the optimal constants. As can be seen in Figure 51, the existing data is full of jitter, that can be seen in green. The data in blue on the plant is what to be achieved.

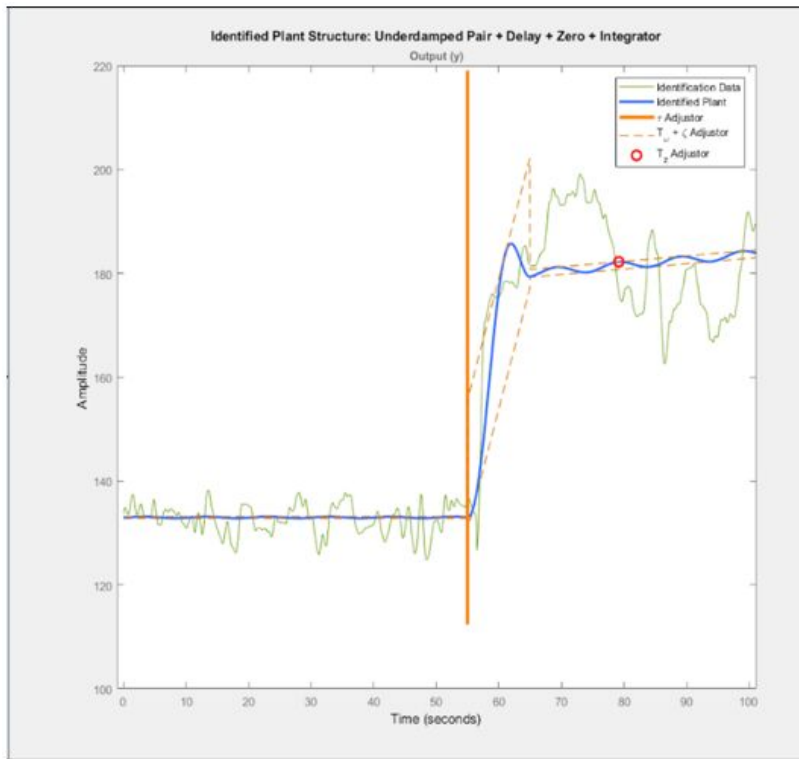


Figure 51. Identified Plant Structure

Using the plant that was developed with the MATLAB 2017b PID Tuner App, it can plot a step response that showed very promising results. From Figure 52, it demonstrated a quick rise time without compromising the amount of overshoot, and the desirable settling time.

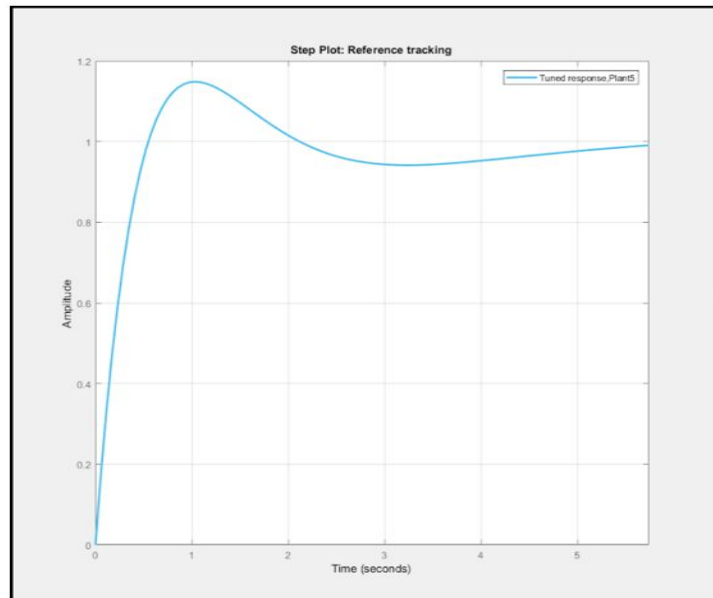


Figure 52. Step Response

Using the Arduino IDE, the PID controller was programmed with the constants from the PID tuner app as shown in Figure 53. The proportional, integral, and derivative gains were -32.8868, -6.8532, and -39.4537. These values yielded very promising results as stated in the previous paragraph. The rise and settling times for the system were 348 milliseconds and 4.47 seconds. Also, the overshoot was not a tremendous amount at 15.9 percent with a peak of 1.16. These values were shown promising result while still maintaining a stable closed loop stability.

Controller Parameters	
	Tuned
Kp	-32.8868
Ki	-6.8532
Kd	-39.4537
Tf	n/a

Performance and Robustness	
	Tuned
Rise time	0.348 seconds
Settling time	4.47 seconds
Overshoot	15.9 %
Peak	1.16
Gain margin	-30.3 dB @ 0.737 rad/s
Phase margin	72 deg @ 4.05 rad/s
Closed-loop stability	Stable

Figure 53. Controller Parameters

6. SUMMARY AND CONCLUSION

In this project, a wind tunnel and Simulink models have been developed. The completion of the wind tunnel has enabled the acquisition of valuable data to test the Simulink models being devised. A simulation interface that can output angle information based on the solar sail size, angle of the paddles, and distance from the Sun was created. From this simulation, it was determined that mechanical actuation produces more effective attitude control than changing reflectivity. These developments made it possible to begin extensive experimentation creating a closed-loop feedback control system in Simulink to perform angle-keeping functions. The objective is to validate a hypothesis that a solar sail mechanical actuation approach similar to the depiction seen below (Figure 54) will be the new, most viable approach to attitude control.

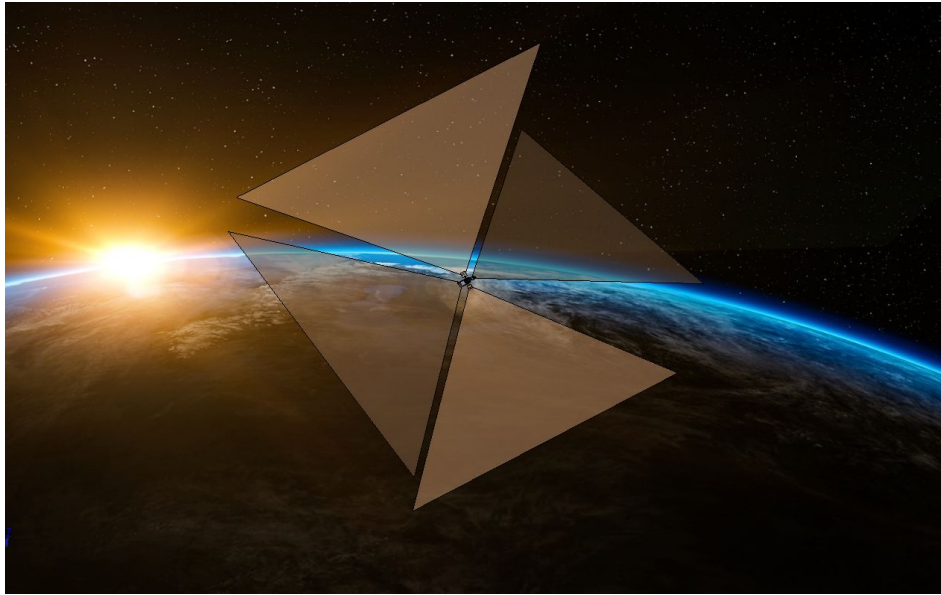


Figure 54. Feathersail, The Next Generation of Nano-Class Sail Vehicles, International Symposium for Solar Sails^[5]

6.1. Broader Social Impact

In 1973, the Mariner 10 probe used its solar arrays to perform solar radiation-powered attitude control during its mission in the inner solar system. In 2004, the MESSENGER probe used solar radiation pressure to perform trajectory corrections around Mercury. Solar sail-based attitude control may be used in a similar manner, exploration of the inner solar system. Just as ocean buoys of, a swarm of CubeSats outfitted with solar sails can function as “solar buoys,” and can provide scientists with a better understanding of solar activity. This novel attitude control method also has several earth-sensing applications, such as possible integrations with polar orbiters in sun-synchronous orbit profiles. Continuous exposure of the solar sails to the sun in such an orbit can enable occasional attitude fixes to be made in a passive, energy-efficient manner.

REFERENCES

- [1] "Arduino Mini 05." *DEV-11303 - SparkFun Electronics*, sparkfun.com/products/retired/11303.
- [2] Banik, Jeremy A, and Thomas W Murphey. *Performance Validation of the Triangular Rollable and Collapsible Mast*. digitalcommons.usu.edu/cgi/viewcontent.cgi?referer=https://www.google.com/&httpsredir=1&article=1193&context=smallsat.
- [3] Bannatyne, Ross. "The Challenges and Evolution of CubeSat Electronics." *Embedded*, www.embedded.com/electronics-blogs/say-what-/4443299/The-challenges-and-evolution-of-CubeSat-electronics.
- [4] Borgnakke, Sonntag, Fundamentals in Thermodynamics. 8 ed, Hoboken, NJ: Wiley, 2013. Print. Ch.3: First Law of Thermodynamics and Energy Equation.
- [5] Alhorn, D.C. "Feathersail – The Next Generation of Nano-Class Sail Vehicle" International Symposium for Solar Sails 2010; 20-22 Jul. 2010; New York, NY; United State, Marshall Space Flight Center (MSFC), Doc ID 20100035087 Huntsville, AL Jul 20, 2010 <https://ntrs.nasa.gov/search.jsp?R=20100035087>.
- [6] Gene Franklin, David Powell, Abbas Emami-Naeni, Feedback Control of Dynamic System, Prentice Hall, 7th Edition.
- [7] Hall, Loura. "Small Spacecraft Technology Program." *NASA*, NASA, 23 Sept. 2015, www.nasa.gov/directorates/spacetech/small_spacecraft/index.html.
- [8] "Heater Flex Circuits, Flexible Heaters." *Flexible Circuits*, www.flexiblecircuit.com/product-category/flexible-heater/.
- [9] Hsu, Jeremy. "Solar Sail Flotilla Could Divert Possibly Dangerous Asteroid." *Space.com*, www.space.com/10531-solar-sail-flotilla-divert-possibly-dangerous-asteroid.html.
- [10] Johnson, Les, et al. "Status of Solar Sail Technology within NASA." *Advances in Space Research*, vol. 48, no. 11, 2011, pp. 1687–1694.
- [11] McInnes, Colin R. *Solar Sailing: Technology, Dynamics and Mission Applications*. Springer Berlin, 2005.
- [12] Munson, Okiishi, Y. Fundamentals of Fluid Mechanics. 4 ed, Hoboken, NJ: Wiley, 2016. Print.
- [13] S. Nadir, Lappas, V. " Deployment System of the CubeSail nano-Solar Sail Mission" Surrey Space Centre, University of Surrey, Guildford GU2 7XH, UK.

- [14] Wall, Mike. "LightSail Solar Sail Prototype Back in Action After Glitch." *Space.com*, www.space.com/29534-lightsail-solar-sail-reboots-after-glitch.html. Accessed 3 Dec. 2017.
- [15] "Sailing to the World's Most Famous Comet." *The Planetary Society Blog*, 2014. [Article]. Available: <http://www.planetary.org/explore/projects/lightsail-solar-sailing/story-of-lightsail-part-1.html>. [Accessed April 13, 2018].
- [16] Society, The Planetary. *Raw video: LightSail solar sail deployment test*. 24 September 2014. May 2018. <https://www.youtube.com/watch?v=AR8TTgq_bRU>.
- [17] Buri, Hani and Yves Weinand. *ORIGAMI-Folded Plate Structures, Architecture*. 2008.
- [18] Fu, Sperber, & Eke. (2016). Solar sail technology—A state of the art review. *Progress in Aerospace Sciences*, 86, 1-19.
- [19] Harkness, Mcrobb, Lützkendorf, Milligan, Feeney, & Clark. (2014). Development status of AEOLDOS – A deorbit module for small satellites. *Advances in Space Research, Advances in Space Research*.

APPENDIX

Table A-1. Contract Work Breakdown Structure.

CWBS	Task	Lead
1.0	Phase I - Requirements and Concept Design	
1.1	Propulsion Selection	Dongling
1.2	Attitude Control Strategy	Dennis
1.3	Preliminary Calculations	Yosuar
1.4	Structures/ Deployable	Steve
1.5	Design Trades	Kevin
1.6	Establish System Requirements	Dennis
1.7	Concept Design Review	Paolo
2.0	Phase II: Preliminary Design	
2.1	Hardware Architecture	Kevin
2.2	Software Architecture	Paolo
2.3	Drawings	Yosuar
2.4	Control Simulations	Paolo
2.5	Preliminary Budgets	Dongling
2.6	Flow Diagram Verification	Yosuar
2.7	Preliminary Design Review	Steve
3.0	Phase III - Detail Design, Fabrication, and Assembly	
3.1	Subsystems Interface Analysis	Yosuar
3.2	Testbed Fabrication	Steve
3.3	Component Assembly	Kevin
3.4	PC Boards Integration	Dennis

4.0	Phase IV: Test and Evaluation	
4.1	Unit Testing	Dennis
4.2	Data Acquisition	Steve
4.3	Component, Environmental Functional Analyses	Paolo
4.4	Final Budgets	Dongling
4.5	Final Design Review	Dennis
5.0	Program Management	
5.1	Systems Engineering Management	Steve
5.2	Technical Management	Kevin
5.3	Budget Management	Dongling
5.4	Reviews	All